SCFT study of nonfrustrated ABC triblock copolymer melts

ARTICLE *in* MACROMOLECULES · JUNE 2007

Impact Factor: 5.8 · DOI: 10.1021/ma062778w

SCFT Study of Nonfrustrated ABC Triblock Copolymer Melts

Christopher A. Tyler, Jian Qin, Frank S. Bates, and David C. Morse*

Department of Chemical Engineering and Materials Science, University of Minnesota, Minneapolis, Minnesota 55455

Received December 4, 2006; Revised Manuscript Received April 11, 2007

ABSTRACT: The phase behavior of ABC triblock copolymer melts is studied by self-consistent-field theory (SCFT). We focus on "nonfrustrated" triblocks, in which the Flory−Huggins interaction parameter χ_{AC} between the end blocks is significantly larger than that between the middle and either end block, i.e., $\chi_{AC} \gg \chi_{AB} \sim \chi_{BC}$. Such systems tend to form ordered structures with no AC interface. Complete phase triangles at fixed values of the products $\chi_{ij}N$ are presented for a model with $\chi_{AB} = \chi_{BC} \ll \chi_{AC}$ and for a model with parameters chosen to represent poly(isoprene-*b*-styrene-*b*-ethylene oxide) copolymers that have recently been studied experimentally. Particular attention is paid to the structure of the orthorhombic O^{70} network phase and the reasons for its existence as well as to the sensitivity of the predicted phase behavior to changes in the χ parameters.

1. Introduction

SCFT provides a particularly simple description of the phase behavior of AB diblock copolymer melts. It predicts that the phase behavior of any neat AB diblock copolymer depends only upon the volume fraction f_A of the A block, the product χN of the Flory−Huggins χ parameter and the chain length N, and (in general) the ratio of statistical segment lengths. In contrast, ABC triblock copolymer phase behavior is governed by no fewer than five parameters, even if we neglect differences in statistical segment lengths: two independent volume fractions, f_A and f_B, and the products $\chi_{AB}N$, $\chi_{AC}N$, and $\chi_{BC}N$ of the chain length with three different Flory−Huggins parameters. It will be impossible to exhaustively search all possible points in this parameter space in a manner analogous to that completed for AB diblocks and much more difficult to grasp universal principles of phase behavior in ABC triblocks.

As a step toward taming this complexity, Bailey[1] suggested a division of triblock copolymer melts into three categories according to the relative magnitude of χ_{AC}, the interaction between the end blocks, compared to that of χ_{AB} and χ_{BC}, the interaction between neighboring blocks. (We may always choose monomer labels such that $\chi_{BC} \geq \chi_{AB}$, as a matter of convention.) The three types correspond to systems in which χ_{AC} is bigger than, smaller than, and intermediate between χ_{AB} and χ_{BC}. The three types of systems are distinguished by the cost of A/C interfacial contact. Because A/C contacts are not imposed by the connectivity of the linear ABC molecule, A/C interfaces form only when they are energetically favored, whereas A/B and B/C interfaces are required by the molecular architecture. Bailey referred to systems in which A/C interactions are less thermodynamically expensive than A/B or B/C interactions as *frustrated*.[1] Bailey denoted systems in which the A/C interaction is less costly than either of the other interactions, so that $\chi_{AC} < \chi_{AB} < \chi_{BC}$, as F^2 systems, which are said to have type II frustration. Systems in which χ_{AC} is intermediate between the other interaction parameters, i.e., $\chi_{AB} < \chi_{AC} < \chi_{BC}$, are denoted F^1 systems and are said to have type I frustration. When the A/C interaction is more expensive than either A/B or B/C interactions, the system is an F^0 system and is said to have no frustration.

Systems with type II frustration, in which the interaction between end blocks is the smallest of the three interactions, tend to exhibit novel decorated phases, such as spheres on spheres, spheres on cylinders, rings on cylinders, and cylinders in lamellae. The morphologies observed in these systems minimize the area of A/B and B/C interfaces by isolating the B domains into spheres, cylinders, or rings, at the expense of the formation of larger areas of A/C interface. Many systems in this class have now been characterized: poly(styrene-*b*-ethylpropylene-*b*-methyl methacrylate) (PS−PEP−PMMA) by Stadler and co-workers[2−6] and by Abetz and co-workers,[7] poly(styrene-*b*-butadiene-*b*-methyl methacrylate) (PS−PB−PMMA) by Stadler and co-workers,[3−6,8,9] and poly(styrene-*b*-butadiene-*b*-caprolactone) (PS−PB−PCL) by Balsamo and co-workers.[10]

Systems with no frustration, or F^0 systems, in which χ_{AC} is the largest of the three interaction parameters, form structures with no A/C interface. Among such structures are core−shell versions of those observed in diblocks, including core−shell spheres, cylinders, gyroid, and lamellae, and alternating versions of the sphere, cylinder, and gyroid phases, in which the A and C domains form alternating equivalent sublattices within a B matrix. In addition, such systems have been observed to form two orthorhombic network phases (with space groups *Fddd* and *Pnna*) that are not analogous to any of the four well-established equilibrium phases of diblock copolymers. Systems of this class that have been characterized experimentally include poly(butadiene-*b*-styrene-*b*-vinylpyridine) (PB−PS−PVP) and poly(methyl methacrylate-*b*-styrene-*b*-butadiene) (PMMA−PS−PB) by Abetz and co-workers,[11,12] poly(isoprene-*b*-styrene-*b*-vinylpyridine) (PI−PS−PVP) by Matsushita and co-workers,[13−15] and poly(isoprene-*b*-styrene-*b*-ethylene oxide) (PI−PS−PEO) by Bailey, Epps, Bates, and co-workers.[16−18]

Systems with type I frustration, in which the interaction between end blocks is of intermediate strength, span a range of structures between those observed in F^2 systems and those observed in F^0 systems. Observed phases include alternating spheres on a BCC lattice, as observed in a CsCl crystal, core−shell gyroid, core−shell cylinders, perforated-lamellar, and pillared-lamellar. Studied systems include poly(styrene-*b*-isoprene-*b*-ethylene oxide) (PS−PI−PO) by Bailey et al.,[1] poly(styrene-*b*-butadiene-*b*-vinylpyridine) (PS−PB−PVP) by Abetz and co-workers,[11,19] poly(styrene-*b*-isoprene-*b*-vinylpyridine) (PS−PI−PVP) by Matsushita et al.,[20] and poly(isoprene-*b*-styrene-*b*-dimethylsiloxane) (PI−PS−PDMS) by Shefelbine et al.[21]

10.1021/ma062778w CCC: $37.00
Published on Web 06/05/2007

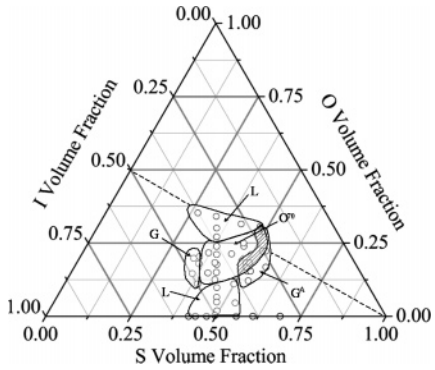

Figure 1. Partial phase map of poly(isoprene-*b*-styrene-*b*-ethylene oxide), or ISO, in the vicinity of the order−disorder transition for temperatures ranging from 100 to 225 °C. The observed phases include 2- and 3-domain lamellae (*L*), gyroid (*G*), orthorhombic network (O^{70}), and alternating gyroid (G^A). The open dots represent the different polymers that were synthesized and characterized to locate the phase boundaries. The solid lines is added for guidance. The hatched domain denotes a window in which an order−order transition from O^{70} to G^A with increasing temperature was observed. Adapted from Epps et al.[17]

In the remainder of this paper, we focus on "nonfrustrated" or F^0 systems. Two systems of this type have been particularly extensively studied: PI−PS−PVP by Mogi, Matsushita, and co-workers[13−15] and PI−PS−PEO by Bailey, Epps, Bates, and co-workers.[16−18] Mogi, Matsushita, and co-workers systematically explored the phase map of a set of PI−PS−PVP triblocks with $f_A \simeq f_C$. They observed morphological transitions from lamellae to alternating gyroid, alternating cylinders, and alternating spheres, with increasing f_B. Bailey, Epps, Chatterjee, Bates, and co-workers[16−18] have systematically explored the parameter space of system PI−PS−PEO, which is referred to hereafter as ISO. By using a PI−PS diblock as a macroinitiator, they synthesized several sequences of ISO triblock copolymers with a fixed ratio of f_A to f_B and with increasing f_C. They identified three network phases: a core−shell gyroid network, an alternating gyroid network, and a newly discovered, orthorhombic, birefringent network with space group *Fddd* (number 70). This orthorhombic phase, which was initially observed along the $f_A = f_B$ isopleth from $f_C = 0.12-0.26$, denoted O^{70}, can be visualized as a network of 3-fold connectors with a local structure similar to that found in the core−shell gyroid phase but arranged on an orthorhombic unit cell. The phase is directly accessible from the disordered phase upon cooling. The work of Epps et al.[17] demonstrated that the phase occupies a substantial region of the ISO phase triangle near the order−disorder transition. Their partial phase triangle is reproduced in Figure 1. It contains lamellae and the three distinct network phases. A more complete phase map for this system was recently published by Chatterjee et al.[18]

Cochran and Bates[22] have also identified a different nonequilibrium orthorhombic network structure in poly(cyclohexane-*b*-ethylethylene-*b*-ethylene), or hydrogenated PS−PB−PI, which is also an F^0 system. At equilibrium, a sample with volume fractions $f_A = f_C = 0.25$ and $f_B = 0.50$ was found to form an O^{70} phase. Upon exposure to large-amplitude oscillatory shear, it is found to evolve into a distinct orthorhombic network, also composed of 3-fold connectors, with space group *Pnna* (number 52), denoted O^{52}.

Several theoretical studies of linear ABC triblock copolymer melts have relied on different approximate strong-segregation theories.[3,23−25] Both Nakazawa and Ohta[23] and Zheng and Wang[24] considered the strong-segregation limit of a density-functional theory similar to that developed by Ohta and Kawasaki[26,27] to describe diblock copolymer melts. Nakazawa and Ohta considered the competition between lamellar, alternating spheres (i.e., CsCl), alternating cylinders, and a somewhat crude approximation for an alternating diamond network, in systems with $f_A = f_C$ and $\chi_{AB} = \chi_{AC}$. These authors were the first to show that the preferred packing of alternating A and C cylinders in an ABC triblock melt with immiscible A and C blocks corresponds to a square unit cell, with A cylinders at the origin and C cylinders at the center, rather than to a hexagonal packing. Zheng and Wang conducted a broader survey of the phase behavior of ABC triblocks. They constructed coarse phase maps as functions of compositions for six sets of χ parameters, including representatives of the F^0, F^1, and F^2 classes, while considering 11 candidate phases (lamellae, cylinders, spheres, alternating spheres, and several decorated phases) but no network phases. Stadler et al.[3] and Phan and Fredrickson[25] have considered other forms of strong segregation theory, and both also predicted a square unit cell for the alternating cylinder phase.

The only previous systematic numerical SCFT study of ABC triblock melts that allowed for three-dimensionally periodic structures, prior to a brief report of the work discussed here,[28] was a study by Matsen[29] of symmetric triblocks with $\chi = \chi_{AB} = \chi_{BC}$ and $f_A = f_C$. Matsen provided detailed calculations for systems with $\chi_{AC} = \chi$ with $\chi N = 0-80$ and for $\chi N = 50$ with $\chi_{AC}/\chi = 0.0-2.0$. He did not consider any decorated phases but did consider gyroid, alternating gyroid, and alternating diamond networks as well as lamellar, alternating sphere, and alternating cylinder phases. Matsen's work was motivated in part by experimental work by Matsushita and co-workers[13−15] on PI−PS−PVP copolymers with equal volume fractions of PI and PVP. This theoretical study lead to the proper identification of the alternating-gyroid phase in these experiments, which Matsushita et al. had initially misidentified as a triply continuous (or alternating) diamond phase.

Two groups[30−32] have also reported ABC triblock copolymer phase diagrams constructed by numerically solving the SCFT equations in two dimensions. Several lamellar and cylindrical phases were found to be stable, including both alternating and core−shell cylinder phases, two and three domain lamellar phases, and various decorated lamellar phases.

Erukhimovich has constructed a weak-segregation (WS) theory for ABC triblocks,[33,34] analogous to Leibler's[35] weak-segregation theory of diblock copolymer melts. Erukhimovich's theory, like Leibler's, is rigorously valid only near a critical point at which the order−disorder transition is continuous. Erukhimovich showed how the location of critical points within the composition triangle of an ABC system could be identified by searching the spinodal surface for "critical lines". Critical lines are lines along which the third derivative of the free energy with respect to the amplitude of the critical fluctuation mode vanishes. He noted that in thermodynamically symmetric systems, with $\chi_{AB} = \chi_{BC}$ and equal segment lengths $b_A = b_B = b_C$, the isopleth $f_A = f_C$ is a critical line as a result of a symmetry with respect to relabeling of A and C monomers. Erukhimovich focused on systems in which the χ parameters satisfy the Hildebrandt (i.e., solubility parameter) approximation, in which $\chi_{ij} \propto (\delta_i - \delta_j)^2$, where δ_i is a solubility parameter for monomer *i*. He gave detailed numerical results for the phase diagram only for unfrustrated symmetric systems, with $\chi_{AB} = \chi_{BC}$ and $\chi_{AC} = 4\chi_{AB}$, for which there is always a potential critical point somewhere along the $f_A = f_C$ line. (We refer to this as a "potential" critical point because the weak-segregation theory

Table 1. Candidate Phases Considered in the Calculation of the SCFT Phase Maps, with the Hermann−Mauguin Symbol and Space Group Number

phase	Hermann−Mauguin symbol	space group number	description
D			disordered melt
L	-		lamellar
C	$p6mm$	17 (2d)	hexagonally packed cylinders
G	$Ia\bar{3}d$	230	double-gyroid network
S	$Im\bar{3}m$	229	BCC spheres
PL_{ab}	$P6_3mmc$	194	*ab*-stacked perforated lamellae
PL_{abc}	$R\bar{3}m$	166	*abc*-stacked perforated lamellae
C^A	$p2mm$	6 (2d)	alternating cylinders
G^A	$I4_132$	214	alternating gyroid network
S^A	$Pm\bar{3}m$	221	alternating spheres/CsCl structure
Q^{228}	$Fd\bar{3}c$	228	double-diamond network
Q^{227}	$Fd\bar{3}m$	227	alternating diamond network
O^{52}	$Pnna$	52	noncubic (10,3)-*d* network[38]
O^{70}	$Fddd$	70	noncubic (10,3)-*c* network[38]

cannot exclude the possibility that a predicted continuous transition could be preempted by a discontinuous transition.)

In the present work, numerical SCFT calculations are carried out for ABC triblocks with $\chi_{AC} \gg \chi_{BC} \approx \chi_{AC}$. Complete phase map triangles are constructed for two models with fixed values of the statistical segment lengths, the χ parameters, and total degree of polymerization N, but variable copolymer composition. The first is a symmetric system with equal statistical segment lengths and $\chi_{AB} = \chi_{BC}$. The second is a slightly asymmetric system in which we use published values for the statistical segment lengths and the binary χ parameters appropriate to ISO. In addition, the phase map of an idealized diblock copolymer is reexamined, while allowing for O^{70} phase in addition to those considered previously by Matsen and Schick.[36]

2. Methodology

The SCFT phase maps of triblock copolymer melts are determined by comparing the free energies of a large set of candidate phases that have been observed or hypothesized in diblock copolymers or similar ABC triblock systems. The free energy for each phase is minimized with respect to variations in the unit cell parameters with the variable-unit-cell algorithm reported by Tyler and Morse.[37]

Thirteen candidate phases are considered in our calculation, as listed in Table 1. The candidate phases include those previously found to be stable (L, C, G, S) for diblock copolymers, PL_{ab}, PL_{abc} perforated lamellar structures, double diamond (Q^{228}), and alternating versions of the sphere (S^A), cylinder (C^A), gyroid (G^A), and diamond (Q^{227}) phases. In addition, we include the two recently observed orthorhombic networks, O^{70} and O^{52}. The label of each phase is adopted either from the literature on the phase behavior of diblock copolymers, e.g., L, C, S, or from the convention of the surfactant literature, denoting the crystal system and space group number; e.g., O^{70} is an orthorhombic phase with space group number 70, and Q^{227} is a cubic phase with space group 227. A superscript A is used to indicate an alternating phase with two topologically similar sublattices of A and C. The alternating cylinder (C^A) phase in our calculation is based on a rectangular unit cell in which the unit cell lengths a and b can vary independently. This can reproduce either a hexagonal packing, with $b = \sqrt{3}a$, or the alternating square packing, with $b = a$, that other authors (see, e.g., Matsen[29]) have referred to as a "tetragonal" cylinder phase.

No decorated phases, such as rings on cylinders or spheres in cylinders, have been considered. Such phases are primarily observed in F^2 systems where the largest interactions are those between neighboring A and B or B and C blocks.[1] Because we consider only F^0 systems, we do not expect this omission to affect our results.

We have also briefly considered two novel phases proposed by Erukhimovich:[34] the BCC_3 phase (space group $Im\bar{3}m$) and the G_2 phase (space group $I\bar{4}3d$). Erukhimovich's weak-segregation theory predicts these phases to be stable in a two-wavenumber approximation in both diblock and ABC triblock melts,[34] but only for conditions that are sufficiently far from the critical point that the validity of a weak-segregation theory is questionable. The proposed BCC_3 phase is a structure with the same space group as the usual BCC phase, but in which the strongest modulation of monomer concentration, corresponding to the primary peaks in scattering, occurs for the {211} rather than the {110} family of reciprocal lattice vectors. We have successfully converged BCC_3 structures for diblock copolymer melts by numerical SCFT in the region of parameter space in which the two-wavenumber weak-segregation theory predicts this phase to be stable but found that it is actually never the phase of lowest free energy. We believe that the predicted stability of this phase is a result of the use of weak-segregation theory outside its range of validity, a possibility that Erukhimovich acknowledged.[34] We have also attempted to construct solutions with the proposed space group $I\bar{4}3d$ of the G_2 solution, which is a subgroup of the $Ia\bar{3}d$ space group of the gyroid phase. We find that these solutions always converge to a gyroid solution. We also find, however, that the phase relations among plane waves given by Erukhimovich in his description of the G_2 phase are incompatible with space group $I\bar{4}3d$, suggesting that the space group was misidentified. We have thus not included either BCC_3 or G_2 structures among the candidate phases in our phase diagram calculations.

The SCFT-modified diffusion equation for a single chain can be solved either with a fully spectral method, as done by Matsen and Schick,[36] or with the pseudo-spectral method, which was introduced in the context of polymer SCFT by Rasmussen and Kalosakas.[39] Both methods have been used in this work and give equivalent results: we began the project with a fully spectral method similar to that of Matsen and Schick and implemented a pseudo-spectral algorithm during the course of the research. In both implementations, we impose a specified space group symmetry by expanding functions of position in terms of basis functions with the desired space group symmetry. Our implementation of the pseudo-spectral method combines the "time-stepping" algorithm of Rasmussen and Kaloskas with the Richardson extrapolation with respect to step size to achieve higher accuracy. In our implementations, the spectral method remains faster than the pseudo-spectral method in crystals with a large point group (e.g., the cubic G and S phases) when a moderate number ($\lesssim$300) of symmetrized basis functions are required, while the pseudo-spectral method becomes more efficient in phases with less symmetry (e.g., O^{70}) and when a larger number of basis functions are required to achieve the desired precision. In subsequent calculations on more strongly segregated structures, we plan to use the pseudo-spectral method exclusively.

3. ABC Triblocks with $\chi_{AB} = \chi_{BC}$

We first consider an idealized model of ABC triblock copolymers with equal statistical segment lengths for all blocks and equal interaction strength between neighboring blocks, i.e., $\chi_{AB} = \chi_{BC}$. We consider a set of systems with variable volume fractions for each block but fixed interaction parameters of

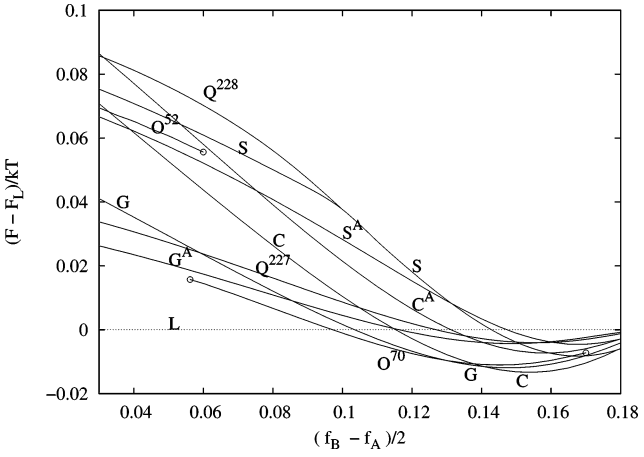

Figure 2. SCFT free energy of various candidate phases, relative to that of the lamellar phase, along the $f_C = 0.16$ isopleth in an idealized triblock copolymer. The stable phases are, from left to right, *L*, O^{70}, *G*, *C*, and *S*. The open circles for O^{70} and O^{52} denote limits of stability (see detailed discussion in text).

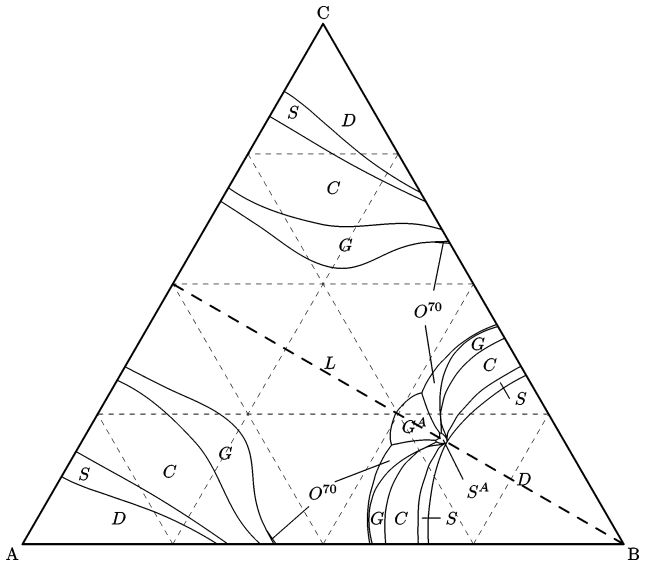

Figure 3. SCFT phase behavior of an idealized triblock copolymer with equal statistical segment lengths for each block and with $\chi_{AC}N = 35$, $\chi_{AB}N = \chi_{BC}N = 13$. The phase map is symmetric across the $f_A = f_C$ isopleth, shown as a dashed line.

$\chi_{AB}N = \chi_{BC}N = 13$ and $\chi_{AC}N = 35$. This is a rough approximation to ISO, with the important difference that, in the idealized system, we neglect the small differences between χ_{AB} and χ_{BC}.

A two-dimensional phase map for each set of systems of variable composition has been constructed by calculating free energies of all the candidate phases along a set of lines of constant f_A, f_B, or f_C, while holding χ parameters, segment lengths, and overall degree of polymerization constant. An example of one such cut through the phase triangle is shown in Figure 2, where we show the free energy per molecule of each candidate phase, relative to the free energy of the lamellar phase, along a line of constant $f_C = 0.16$ for $0.45 < f_B < 0.60$. The free energy of the PL_{ab} phase is not shown because it is substantially higher than that of the other candidate phases. The numerical errors for the free energy are much smaller than the thickness of the lines. Note the small absolute scale for the free energy difference: differences in free energies of closely competing phases (e.g., *G* and O^{70}) are often of order $(10^{-3}-10^{-2})k_BT$ per polymer. Along this line through the phase triangle, the phase sequence with increasing f_B is $L \rightarrow O^{70} \rightarrow G \rightarrow C \rightarrow S$, with the $C-S$ boundary near the right-hand edge of the figure.

The O^{70} and O^{52} orthorhombic network phases are found to be mechanically stable over only limited ranges of parameters. The open circles shown in Figure 2 denote limits of stability of these phase. Beyond these points, we are unable to find SCFT solutions in an equilibrium unit cell by continuation of stable solutions found at nearby parameters. To understand this instability, we calculated the second derivatives of the free energy with respect to the unit-cell parameters *a*, *b*, and *c*; i.e., we have calculated the derivatives of the stress, which are related to the elastic moduli of the crystal. We find that these limits of numerical stability occur at parameters for which one of the eigenvalues of the matrix $\partial^2F/\partial\theta_i\partial\theta_j$ approaches zero, where θ_i is one of the unit cell parameters *a*, *b*, or *c*. Thus, these numerical instabilities coincide with true mechanical instabilities. In the O^{70} phase, the instability never occurs in a region where O^{70} is the preferred structure. The instability is nearly doubly degenerate, with unstable eigenvectors that correspond approximately to extension along the *b* and *c* axes at constant *a*.

Free energies for some candidate space groups are not shown in Figure 2 because they are found to yield structures equivalent to those obtained from other higher symmetry space groups. The PL_{abc} hexagonal phase is not shown because it is found to converge to a structure identical to that obtained for the Q^{227} alternating diamond phase. That is, the optimal unit cell that we obtain from a converged solution of the variable-unit-cell algorithm for PL_{abc} yield a structure that actually has the full cubic symmetry of the diamond Q^{227} space group, which is supergroup of the $R\bar{3}m$ space group of the PL_{abc} structure. The simplest analogue of this phenomenon would be if the optimal choice of the *a*, *b*, and *c* unit cell lengths in a system upon which we imposed an orthorhombic space group were found to be equal, yielding a cubic crystal. Similarly, at $(f_B - f_A)/2 \approx 0.1$, the optimal double diamond (Q^{228}) and BCC (*S*) phases are found to become equivalent.

Figure 3 shows the full phase triangle obtained for this set of molecules, identifying compositions in which each phase is stable. Figure 4 is a more detailed view of a complex region in the B-rich corner that contains the alternating gyroid (G^A) and alternating sphere (S^A) phases. The phase triangle is symmetric about the line $f_A = f_C$, shown as a dashed line, as a result of our use of symmetric interaction parameters, $\chi_{AB} = \chi_{BC}$. The only phases that are found to be stable somewhere within this phase triangle are those that were previously known to be stable in diblock copolymers (i.e., *D*, *S*, *C*, *G*, and *L*) and the G^A, S^A, and the O^{70} network phases. For this set of parameters, we find no regions where any of the other candidate phases are stable.

The phase map is dominated by a large lamellar region, which extends to the middle of each of the binary edges. Within this region, there is a continuous evolution from a "two-color" structure along each of the edges to a "three-color" structure near the middle of the phase triangle, in which A, B, and C form well-segregated layers.

The sphere, cylinder, and gyroid phases form continuous arcs across the A- and C-rich corners of the triangle, where one of the end blocks is the majority component. In the A- and C-rich corners, these are all core−shell structures. In the A-rich corner, each of these structures contains a C core surrounded by B shell in a A matrix, with the reverse (A core/B shell/C matrix) in the C-rich corner. The continuous arcs formed by the phases in the phase triangle reflect a continuous evolution in the volume fractions of the core and shell blocks. For example, consider the evolution of structure along a path within the sphere phase

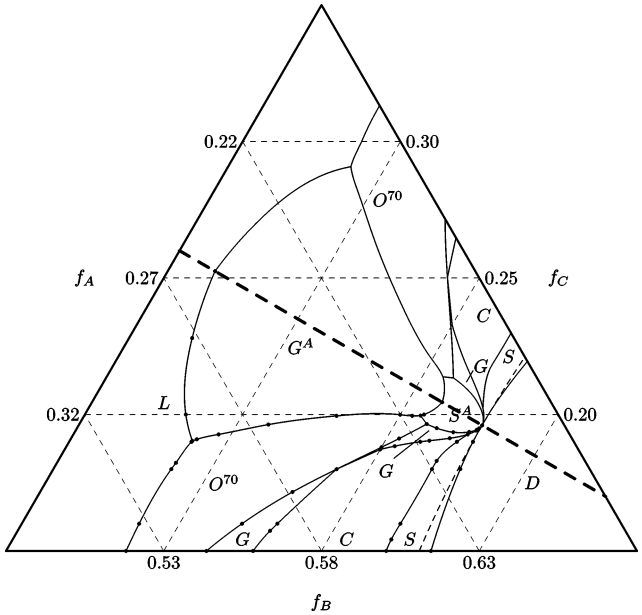

Figure 4. Expanded view of the region of the phase map near the critical point for the idealized triblock copolymer ($\chi_{AC}N = 35$, $\chi_{AB} = \chi_{BC}N = 13$), for $f_A = 0.17-0.37$, $f_B = 0.48-0.68$, and $f_C = 0.15-0.35$. Dots denote the points at which we have calculated the phase boundaries. The light dashed curve that is tangent to the order disorder transition at the critical point is the spinodal of the disordered phase, calculated with the RPA.

in the A-rich corner, traversed from the AB edge, where the structure contains B spheres in an A matrix, to the AC edge. As a C block of increasing length is added to the end of the B, a spherical "core" of C grows in the middle of each sphere, while the volume fraction of the surrounding shell of B shrinks, until a structure of C spheres in an A matrix is obtained at the AC edge. An analogous change in the volume fractions of the "core" and "shell" components occurs in the cylinder and gyroid phases in both the A- and C-rich corners.

The phase behavior in the B-rich corner is more complicated. Here, regions in which the sphere, cylinder, gyroid, and O^{70} phases are stable near the AB and CB edges are separated by alternating sphere and alternating gyroid phases, which appear near the isopleth $f_A = f_C$. Note that the regions on either side of this isopleth in which an O^{70} phase is stable become wider, and the regions of gyroid stability become narrower, as the $f_A = f_C$ line is approached from either side.

Consider the structural evolution within (for example) the sphere phase along a path that starts from the AB edge, where the structure is a lattice of A spheres in a B matrix, toward the $f_A = f_C$ isopleth. Along this path, a C block is added to the end of the B matrix block, while the length of the A core block decreases. Because a minority C block is added to the end of the matrix block along this path, C monomers must segregate into C-rich pockets within the B matrix, rather than within the spherical A-rich domains. In both the sphere and cylinder phases, C tends to segregate near the interstitial sites. These are arranged on the face centers of the cubic lattice in the BCC sphere phase and on a honeycomb lattice in the hexagonal cylinder phase.

The *S*, *C*, *G*, and O^{70} phases that form in the region $f_C < f_A < f_B$ near the AB edge thus all have "core" domains of A in a matrix of B, within which C segregates preferentially into what we will refer to as "interstitial" domains. The distinction between "core" and "interstitial" domains is admittedly arbitrary when both are minority domains. By convention, however, we will refer to the domains that resemble those of the corresponding diblock copolymer phases as the "core" domains. The "interstitial" domains into which C monomers must segregate may be either disconnected pockets surrounding interstitial sites, as occurs the *S* and *C* phases when f_C is small, or they may evolve into multiply connected domains, as occurs in the *G* and O^{70} phases for larger values of f_C. In the *S*, *C*, *G*, and O^{70} phases, however, the interstitial domains are all geometrically distinct from the core domains. As a result, we find that the solutions to the SCF equations that correspond to the core−matrix−interstitial structures found for $f_B > f_A > f_C$, which have A core domains, cannot be continuously evolved, by changing composition in small increments, into the corresponding structures found in the region $f_B > f_C > f_A$, which have C core domains and A interstitial domains.

Near the $f_A = f_C$ isopleth, we find alternating gyroid and sphere phases, in addition to the disordered and lamellar phases. In these alternating phases, unlike those discussed above, the A and C domains are topologically similar and become identical (aside from a relabeling of A and C monomers) along the line $f_A = f_C$.

It was not initially clear to us whether the O^{70} phase could be considered an "alternating" phase, with topologically similar *A* and *C* domains, in the same sense as the alternating gyroid phase. We find, however, that the O^{70} SCF solutions obtained at $f_A = f_C$ by continuously evolving the equilibrium structure found for $f_C < f_A$ is different from that obtained from continuing the solution found for $f_C > f_A$. When $f_A = f_C$, we thus obtain two distinct O^{70} structures of the same free energy, both of which have geometrically inequivalent A and C domains. We also find that it is possible to obtain a third alternating O^{70} solution in which the A and C domains actually are equivalent, for which the structure is invariant under relabeling of A and C and a shift by 1/2 unit cell along the *c* direction. This "alternating" O^{70} structure is, however, never the minimum free energy solution with *Fddd* space group symmetry.

Interestingly, we find that equilibrium O^{70} structure found on the C-rich side of the B-rich corner ($f_A < f_C < f_B$) *can* be continuously evolved into a metastable O^{70} network in the A-rich corner. This structure, which has a core C-rich network domain, is stable in the A-rich corner for the parameters considered here only within a very small sliver between *G* and *L* near the AB edge, though it is nearly stable along much of the *G*−*L* phase boundary. This C core network becomes stable throughout a wide band of the phase map predicted for ISO in section 4.

In Figure 3, the regions in which the O^{70} phase is stable in the B-rich corner extend to the AB and CB edges. Because the phase map of an AB diblock with equal statistical segment lengths is symmetric about $f_A = 1/2$, there also exist very small regions of O^{70} stability on the A-rich side of the AB edge and on the C-rich side of the CB edge. The predicted appearance of a stable O^{70} phase in weakly segregated diblock copolymers is discussed in more detail in section 5.

Figures 5−7 depict morphologies of equilibrium *G*, O^{70}, and G^A network phases in the region $f_C < f_A < f_B$ along a line with $f_B \simeq 0.55$. In the *G* morphology shown in Figure 5 at $f_A = 0.33$, $f_B = 0.55$, and $f_C = 0.12$, the C monomers are well mixed with B deep within the matrix, due to the smallness of both f_C and χ_{BC}. The concentration ϕ_C is strongly depleted near the A−B interface, however, due to the large value of χ_{AC}. This can be seen from the similarity of isosurfaces $\phi_B(r) = 0.5$ and $\phi_B(r) + \phi_C(r) = 0.5$, implying that ϕ_C is small near this isosurface. In the O^{70} network shown in Figure 6, for which $f_A = 0.27$, $f_B = 0.55$, and $f_C = 0.18$, C is somewhat more strongly segregated within small C-rich pockets with the B matrix. In the G^A phase shown in Figure 7 for $f_A = f_C = 0.33$, $f_B = 0.55$, and $f_C = 0.12$,

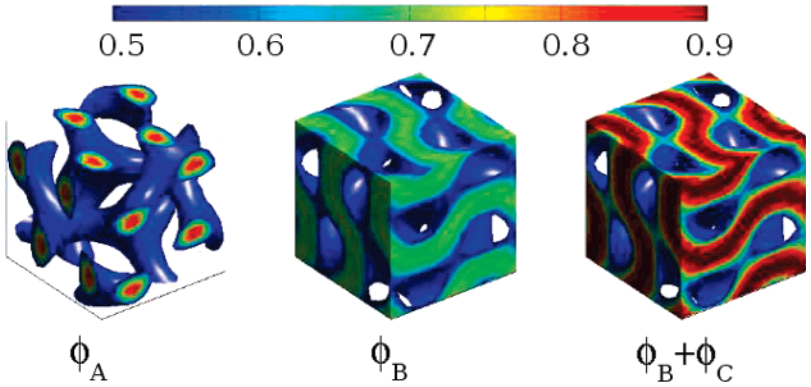

Figure 5. Isosurfaces for ϕ_A, ϕ_B, and $\phi_B + \phi_C$, from left to right, for an idealized triblock copolymer in the *G* phase with $f_A = 0.27$, $f_B = 0.55$, and $f_C = 0.18$. The isosurfaces are shown for a value of 0.50 for each of these volume fractions. The values of the volume fractions within the isosurfaces indicate that B and C monomers are completely mixed deep within the matrix and that the A/B interface is quite diffuse.

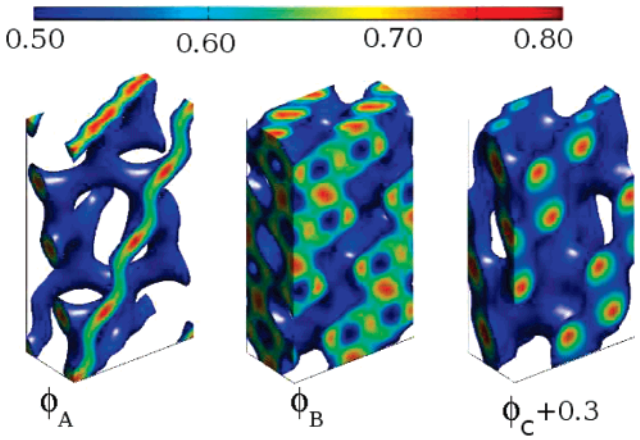

Figure 6. Isosurfaces for ϕ_A, ϕ_B, and $\phi_C + 0.3$, from left to right, for an idealized triblock copolymer in the O^{70} phase with $f_A = 0.27$, $f_B = 0.55$, and $f_C = 0.18$. The isosurfaces are shown at a monomer volume fraction of 0.50.

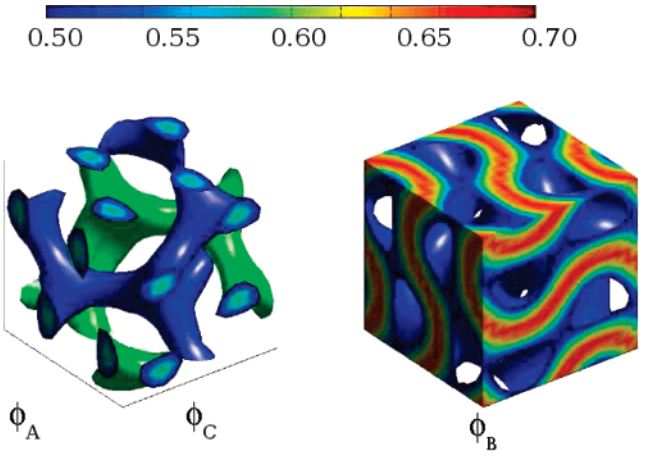

Figure 7. Isosurfaces for ϕ_A (blue, left), ϕ_C (green, left), and ϕ_B (right) for an idealized triblock copolymer in the G^A phase with $f_A = f_C = 0.223$ and $f_B = 0.554$. The isosurfaces are shown at a monomer volume fraction of 0.50. Three distinct domains are evident under these conditions, but the AB and AC interfaces remain quite diffuse.

all three monomer domains are more clearly segregated. However, it is clear from the color scale shown along the edges of the unit cell in these figures that all of the structures produced at such low values of $\chi_{AB}N = \chi_{BC}N$ are rather weakly segregated, with broad interfaces between A- and B-rich regions.

It is apparent from the phase map that *G* and O^{70} networks compete closely in the B-rich corner and that the O^{70} phase is stabilized relative to *G* in the region $f_C < f_A < f_B$ by the addition of a C block to the end of the B matrix block. SCFT can help us understand why one of these networks is favored over another and how the balance is changed by changes in composition or other parameters. For this purpose, it is useful to divide the difference $\Delta F \equiv F^{\alpha} - F^{\beta}$ between the free energies per molecule in two phases α and β into components

$$\Delta F = \Delta F_{AB} + \Delta F_{BC} + \Delta F_{AC} + \Delta F_{chain} \qquad (1)$$

where ΔF_{ij} is the difference in the free energy due to interactions of monomers of types *i* and *j* and ΔF_{chain} is the difference due to the difference in chain conformational entropy, including both chain stretching and the loss of entropy arising from localization of the joints near the interface.[40] Each of the binary interaction free energies is given by a difference $\Delta F_{ij} = F_{ij}^{\alpha} - F_{ij}^{\beta}$, where

$$F_{ij}^{\alpha} = \chi_{ij} N \int \frac{d\mathbf{r}}{V} \phi_i(\mathbf{r})\, \phi_j(\mathbf{r}) \qquad (2)$$

is the *ij* interaction free energy per molecule in phase α, in which the integral is taken over a unit cell of volume *V*.

Table 2 displays the components of the difference $\Delta F^{\alpha\beta}$ for $\alpha = O^{70}$ and $\beta = G$ at a point along the O^{70}–*G* phase boundary and for $\alpha = O^{70}$, $\beta = G^A$ at a point along the O^{70}–G^A phase boundary. Because these values have been evaluated along phase boundaries, where $\Delta F = 0$, the sum of free energy differences either row of this column vanishes, by construction. Columns with negative values thus represent contributions that favor O^{70} (α) over *G* or G^A. We see that O^{70} is favored over *G* by both the CB and CA interactions that involve the minority C block and, for this set of parameters, particularly by the AC interaction. Similarly, G^A is favored over O^{70} by both the CA and CB interactions. This creates a sequence $G \rightarrow O^{70} \rightarrow G^A$ with increasing f_C. The O^{70} network is favored over *G* by increasing f_C because it provides an "interstitial" domain for the C block that does a better job of minimizing interaction between C monomers and both B and A monomers, though it is not as favorable in this regard as the alternating gyroid phase.

It is clear from the entries in Table 2 that ΔF_{AC} plays a significant role in this sequence of transitions between networks. This is a result not only of the comparatively large value chosen for χ_{AC} but also of small values chosen for $\chi_{AB}N = \chi_{BC}N = 13$, which lead to AB and BC interfaces so diffuse that they allow substantial contact between A and C in ordered structures with no AC interface. The AC interaction plays a particularly important role in the G–O^{70} transition in this system because the small C block, with $f_C = 0.150$, is mixed with B within the B-rich matrix in the *G* phase. We expect ΔF_{AC} to become less

Table 2. Components of the Difference between the Free Energies of the O^{70} Network in ABC Triblock and That of the G and G^A Networks, Evaluated at Points along the Phase Boundaries, in Units of k_BT per Molecule[a]

α	β	(f_A, f_B, f_C)	ΔF_{AB}	ΔF_{BC}	ΔF_{AC}	ΔF_{chain}
O^{70}	G^A	(0.252, 0.550, 0.198)	−0.028 691	0.026 441	0.024 500	−0.022 249
	G	(0.300, 0.550, 0.150)	0.008 034	−0.002 613	−0.015 489	0.010 068

[a] ΔF_{AB}, ΔF_{BC}, and ΔF_{CA} refer to the differences in interaction energies of AB, BC, and CA monomer pairs, respectively. ΔF_{chain} is the difference in polymer conformational entropy.

important in systems with larger values of $\chi_{AB}N$ and $\chi_{BC}N$, for which the overlap between A and C will be decreased by the formation of structures with sharper AB and BC interfaces and no direct AC interface.

As predicted by Erukhimovich, the phase map contains a critical point located at the intersection of the symmetry line $f_A = f_C$ and the order−disorder transition in the B-rich corner. For our choice of parameters, this transition lies at $f_A = f_C = 0.196\,05$ and $f_B = 0.607\,90$. The limit of stability of the disordered phase (the spinodal), calculated from the random-phase approximation (RPA), is shown by the dashed line in Figure 4. The phase behavior near this point, at which the sphere, gyroid, and alternating sphere phases converge, is partially analogous to that found near $f = 1/2$ and $\chi N = 10.495$ in diblock copolymers. The order parameters of the stable S, C, and S^A phases and the metastable C^A, G, G^A, and O^{70} phases are all found to vanish continuously at this point.

The explanation of why a critical point should exist along this symmetry line, first given by Erukhimovich,[33,34] is closely analogous to that needed to explain why the critical point in the diblock copolymer copolymer phase map appears at $f_A = 1/2$: the disordered phase of an ABC triblock melt is locally stable when the 3×3 structure function matrix $S_{ij}(\mathbf{q}) = \langle \delta\phi_i(\mathbf{q})\delta\phi_j(-\mathbf{q})\rangle/V$ is positive-definite for all wavevectors $\mathbf{q}$, where $\delta\phi_i(\mathbf{q})$ is a Fourier component of the field $\delta\phi_i(\mathbf{r}) \equiv \phi_i(\mathbf{r}) - f_i$ for monomers of type i, with i = A, B, or C. At the spinodal, one of the eigenvalues of $S_{ij}(\mathbf{q})$ diverges at a critical wave number $|\mathbf{q}| = q^*$. In an incompressible liquid, the spectrum of $S_{ij}(\mathbf{q})$ always contains a compression mode with a vanishing eigenvalue and an eigenvector $(\delta\phi_A,\delta\phi_B,\delta\phi_C) \propto (1,1,1)$. Along the symmetry line $f_A = f_C$, in a system with $\chi_{AB} = \chi_{BC}$ and $b_A = b_B = b_C$, the SCFT free energy $F[\langle\phi\rangle]$ is invariant under a switch in the identities of A and C monomers. As a result, the eigenvectors of $S_{ij}(\mathbf{q})$ must be either even or odd under this symmetry. Because $S_{ij}(\mathbf{q})$ is a real symmetric matrix, they must also be orthogonal to the compression mode and to each other. The two physical eigenvectors along the line $f_A = f_C$ must thus be an even mode $(\delta\phi_A,\delta\phi_B,\delta\phi_C) \propto (1,-2,1)$ (a "B modulation"[34]) and an odd mode $(\delta\phi_A,\delta\phi_B,\delta\phi_C) \propto (1,0,-1)$ (an "AC modulation"[34]). For parameters $\chi_{AC} \gg \chi_{AB} = \chi_{BC}$ of interest here, it is the odd, or AC modulation, mode that becomes unstable at the spinodal. A critical point is a point along the spinodal for which the third derivative of $F[\langle\phi\rangle]$ with respect to the amplitude of the critical mode vanishes. The symmetry of $F[\langle\phi\rangle]$ under interchange of A and C requires that the third derivative of the free energy with respect to the amplitude of the odd mode vanish everywhere along a "critical line" $f_A = f_C$. The corresponding argument for a diblock copolymer melt with $b_A = b_B$ relies upon a symmetry of F with respect to a relabeling of A and B to show that the third-order coefficient must vanish for $f_A = 1/2$.

It is interesting to compare our results, in which we fixed the interaction parameters and varied two independent volume fractions, to those of Matsen,[29] who studied systems with $\chi_{AB} = \chi_{BC}$ and $f_A = f_C$ but varied the parameters $\chi = \chi_{AB} = \chi_{BC}$ and χ_{AC}. Matsen gave detailed results for systems with $\chi = \chi_{AC}$ for a range of values of χN and for systems with $\chi N = 50$ over a wide range of values of χ_{AC}/χ. Over much of the parameter space $\chi_{AC} \geq \chi$, Matsen found a phase sequence $D \rightarrow S^A \rightarrow C^A \rightarrow G^A$ with decreasing f_B. As already noted, our results for $\chi N = 13$ and $\chi_{AC}N = 35$ (which is not among the set of parameters examined by Matsen) do not yield a stable C^A. Unlike us, Matsen did not find a continuous order−disorder transition (ODT) along $f_A = f_C$: He did not mention any continuous ODTs in his publication and confirmed in a private communication that there is no evidence for a continuous transition in his numerical results.

Erukhimovich's analysis[33,34] provides a partial explanation of why Matsen found discontinuous ODT in symmetric ABC triblocks, whereas we find a continuous ODT. As Erukhimovich noted, almost all of the systems studied by Matsen lie in the region of parameter space in which linear stability analysis predicts a B-modulated instability of the disordered phase. The isopleth $f_A = f_C$ is a critical line, however, only for systems that undergo an AC-modulated instability. In systems with sufficiently low values of the ratio $k \equiv \chi_{AC}/\chi_{AB}$ (i.e., $k \lesssim 0.6$ for $\chi_{AB}N = 50$), Matsen found a discontinuous transition to a B-modulated BCC sphere phase, as suggested by this analysis. At intermediate values of this ratio (i.e., $k = 0.6-2.0$ for $\chi_{AB}N = 50$), however, he obtained a discontinuous transition to an AC-modulated alternating sphere (CsCl) phase. It thus appears that a symmetric ABC triblock can undergo a continuous ODT to an AC-modulated phase at large values of k, a discontinous transition to a B-modulated phase at very low values, or a discontinuous transition to an AC-modulated phase at intermediate values of k.

4. ISO Triblock Copolymers

In the idealized system considered in the previous section, we found a stable O^{70} phase that is bordered by L, G, and G^A phases. To this extent, the results agree with the phase behavior observed for ISO by Epps et al.[17] However, in the predicted phase map, the O^{70} phase window is smaller than that observed in experiment and lies far from the $f_A = f_B$ isopleth, where the phase was first observed by Bailey et al.[16] To make a more meaningful comparison of SCFT to the reported phase map for ISO, we next consider a choice of statistical segment lengths and χ parameters that are, as best as we are able to determine, appropriate to ISO.

The choice of literature values for the χ parameters is not straightforward. Two methods are commonly used to measure $\chi(T)$ in diblock copolymer melts: fitting the scattering structure factor in the disordered state to predictions of the random-phase approximation (RPA) and fitting observed order−disorder transitions (ODTs) for symmetric diblocks to the predicted critical value of $\chi N = 10.495$. As discussed by Maurer et al.,[41] these two methods can yield substantially different results for $\chi(T)$. Furthermore, the reported χ values in the literature are often inconsistent even when they are measured with the same method. Table 3 is a compilation of Flory−Huggins parameters for binary interactions of I, S, and O, gleaned from the block copolymer literature.[42−48] All of the displayed values have been converted to a common monomer reference volume of $V_{ref} =$

Table 3. Interaction Parameters $\chi(T) = a/T + b$ and χN at Two Temperatures and at $N = 250$ for Polyisoprene-*b*-polystyrene (IS), Polystyrene-*b*-poly(ethylene oxide) (SO), and Polyisoprene-*b*-poly(ethylene oxide) (IO)[a]

	$\chi(T) = a/T + b$		χN		
	a	b	100 °C $N = 250$	250 °C $N = 250$	reference
IS	22.6	−0.0156	11.2	6.9	Hanley and Lodge[42]
(AB)	26.4	−0.0287	7.5	5.4	Hashimoto et al.[43]
	12.0	0.0086	10.2	7.9	Balsara et al.[44]
	15.7	0.0047	11.7	8.7	Lin et al.[45]
SO	29.8	−0.0229	14.2	8.5	Frielinghaus et al.[46]
(BC)	27.4	0.046	29.9	24.6	Frielinghaus et al.[47]
IO	60.9	0.117	70.1	58.3	Floudas et al.[48]
(AC)	90.0	−0.0579	45.8	28.5	Frielinghaus et al.[46]

[a] The interaction parameters are gleaned from the literature and converted to the values obtained using a reference volume 118 Å^3. The two temperatures represent the lower and upper limit of the experimentally accessible temperature range in ISO. The χ parameters reported by Hanley and Lodge,[42] Hashimoto et al.,[43] Balsara et al.,[44] and Floudas et al.[48] were determined by fitting scattering data to the RPA theory. The values reported by Lin et al.[45] and Frielinghaus et al.[46] were determined by fitting order−disorder transition data to SCFT. The χ values associated with the work of Frielinghaus et al.[47] are our fit to their published ODT data.

118 Å^3. The temperature dependence for each χ_{ij} has been fitted to the form $\chi(T) = a/T + b$. The χ values associated in the table with the work of Frielinghaus et al.[47] are our fit to their published ODT data. The reported χ values for SI agree fairly well at lower temperatures, but there is still a variation of ∼10%. Less data is available for SO and IO, and the reported χ values are considerably less consistent.

Discrepancies in the reported values of χ_{SO} and χ_{IO} leave us considerable freedom in the design of an SCFT calculation. Our goal is to compare the phase behavior predicted by SCFT to the phase behavior measured in the experiments of Bailey, Epps, and co-workers.[16,17] These experiments were conducted for chains of various molecular weights, ranging from $N = 200$ to 300 and over a temperature range of 100−250 °C. We calculate a phase map for a hypothetical set of triblocks with a fixed total chain length of $N = 250$, at a fixed temperature $T =$ 100 °C. We use the smaller of the reported χ parameters at this temperature for both *SO* and *IO* interactions, giving $\chi_{SO}N =$ 14.2 and $\chi_{IO}N = 45.8$, and an average $\chi_{IS}N = 11.0$ of reported values for the *I*/*S* interaction. We use statistical segment lengths $b_I = 6.0$ Å, $b_S = 5.5$ Å, and $b_O = 7.8$ Å for a monomer reference volume of 118 Å^3, which are adapted from published values.[49] This choice of χ parameters is almost, but not exactly, consistent with the Hildebrandt approximation: fixing our values of $\chi_{IS}N$ and $\chi_{SO}N$ while assuming that $\chi_{ij} \propto (\delta_i - \delta_j)^2$ would yield $\chi_{IO}N = 50.2$. To facilitate comparison to the results of this and the previous section, we hereafter use the labels A, B, and C to refer to I, S, and O, respectively.

Figure 8 is the phase triangle for this model of ISO triblock copolymers with fixed values of $\chi_{ij}N$. The O^{70} phase window straddles the $f_A = f_B$ isopleth and is bounded by *G*, *L*, and G^A. With this choice of parameters, the overall SCFT phase map is qualitatively similar to that observed by Epps et al.,[17] as shown in Figure 1. As in the experimental results, the O^{70} window separates a region of "two-color" lamellar order near the line $f_C = 0$, in which C end-block dissolves within B-rich layers, from a "three-color" lamellar region, in which A, B, and C segregate into three more well-defined domains. Like the system with $\chi_{AB} = \chi_{BC}$, this phase map contains a critical point, which is located at a point (0.207 21, 0.643 13, 0.149 66). The location and the phase windows of *L*, O^{70}, *G*, and G^A agree reasonably well with experimental results. The extent of agreement is somewhat surprising in light of the uncertainties in the χ parameters and the sensitivity of the calculated phase map to relatively small changes in these parameters, which is apparent from a comparison of this phase map to that obtained in section 3.

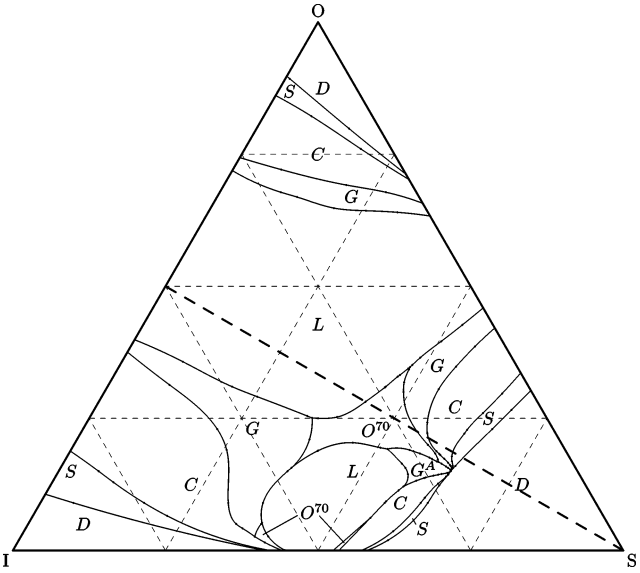

Figure 8. Full phase triangle for a model ISO triblock copolymer, with statistical segment lengths $b_I = 6.0$ Å, $b_S = 5.5$ Å, and $b_O = 7.8$ Å and interaction parameters $\chi_{IS}N = 11.0$, $\chi_{SO}N = 14.2$, and $\chi_{IO}N =$ 45.8.

A close comparison of the SCFT results and experimental results shows some obvious discrepancies, which are worth noting. This calculation fails to predict the experimentally observed phase progression of *G*, O^{70}, G^A with increasing f_B at any fixed f_C (i.e., along any horizontal line in this phase triangle). It also predicts a phase boundary between the O^{70} phase and the "two-color" lamellar region (which extends to the AB edge) at a significantly larger values of f_C than observed experimentally, yielding an O^{70} phase that is stable over a narrower range of f_C than observed experimentally.

Figure 10 shows the predicted structure of an ISO O^{70} phase with $f_A = f_B = 0.395$ and $f_C = 0.21$. In this structure, the C-domain forms a single 3-fold connected network within a matrix of A, while A and C domains are separated by a weakly segregated B-rich shell. At this composition, the structure is most accurately characterized as a core−shell network analogous to the core−shell gyroid that neighbors it in the A-rich corner. Note that the structure shown in Figure 10 is qualitatively different from the O^{70} structure found near the AB edge in the B-rich corner ($f_C < f_A < f_B$) in the model considered in section 3. This structure, shown in Figure 6, contains a core network of A in a matrix of B with weakly segregated pockets of C. The structure shown in Figure 10 is instead similar to the O^{70} structure found near the BC edge in the B-rich corner in section 3, which also contains a core network of C. The change in interaction parameters used to more accurately mimic ISO thus did not cause an expansion of the region of stability of the A core network, which remains stable only very near the AB edge, but instead caused a sequence of C core *G* and O^{70} networks to become stable across a band that connects BC edge to the A-rich corner.

Some insight into why this change in interaction parameters stabilized a C core O^{70} phase can be obtained by again considering contributions to the differences in free energies between competing phases. Table 4 shows components of the differences between the free energy of the O^{70} network found in the region $f_A \sim f_B > f_C$ and those of competing phases. The

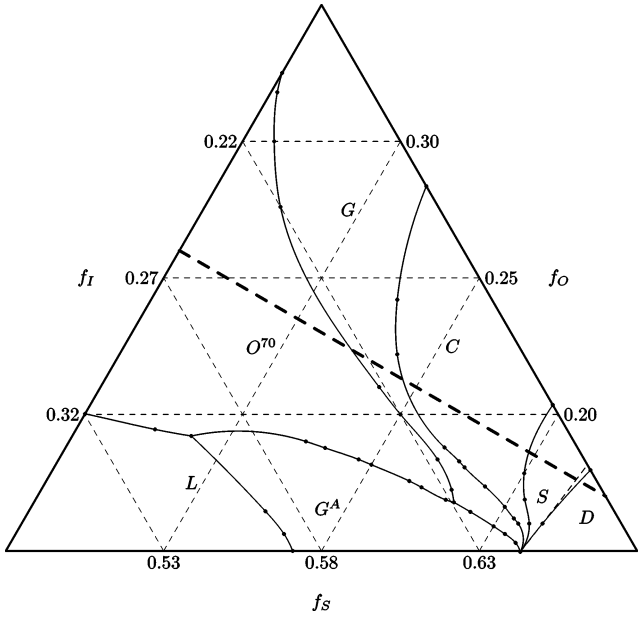

Figure 9. Expanded view of the complex region of the phase map for the ISO triblock copolymer. Dots denote the points at which we have calculated the phase boundaries. The light dashed curve that is tangent to the order−disorder transition at the critical point is the spinodal of disordered phase.

values in each row are evaluated at a point along the phase boundary of the O^{70} and a neighboring phase, as in Table 2. Notice that the O^{70} phase is favored over the lamellar phases along both of the O^{70}−L phase boundaries by a lower BC interaction, while the lamellar phase is favored by a lower AB interaction. Both the increase in $\chi_{BC}N$ from 13 to 14.2 and the decrease in $\chi_{AB}N$ from 13 to 11.2 thus helped stabilize O^{70} relative to L. Conversely, O^{70} is favored relative to a C core gyroid structure along both of its phase boundaries by a favorable AB interaction, while the G phase is favored by a favorable BC interaction. The relationship between the O^{70} and G phases is consistent with that found in the model with $\chi_{AB} = \chi_{BC}$: an ABC triblock O^{70} phase with a core network of C is favored relative to the competing C core gyroid phase by a lower AB interaction energy.

The set of molecules used to calculate Figure 8 is not completely analogous to the set studied by Bailey et al.[16] and Epps et al.[17] In their experiments with ISO, sequences of triblocks with fixed ratios of f_I to f_S were synthesized from a single parent IS diblock. Each such parent diblock was used as a macroinitiator to synthesize a sequence of triblocks with O blocks of increasingly length. For each sequence, the total chain length N thus increased as f_O increased. In the phase maps constructed for both the ISO model of this section and the model of section 3, the total degree of polymerization N was held fixed.

In order to make a more direct comparison to the experiments of Bailey et al.,[16] we have also calculated the free energy of various phases as a function of f_C, for a sequence of molecules in which the length of the C block is increased while keeping the lengths of the A and B blocks fixed. We have considered a sequence of triblocks similar to that studied by Bailey et al., which are grown from a parent diblock with $N = 212$ and $f_A = f_B$, with overall chain lengths ranging from 212 to 318. Figure 11 shows the free energy of the O^{70} phase with reference to the L phase along the $f_A = f_B$ isopleth for $f_C = 0.14-0.40$, corresponding to $N = 240-310$. All other phases have much higher free energies in this region. We find, for this set of molecules, the O^{70} phase is stable for values of f_C from 0.186 to 0.249. This is quite similar to the range of compositions found in the partial phase triangle shown in Figure 8, in which the block copolymer has a fixed chain length $N = 250$, and the O^{70} phase with $f_A = f_B$ is stable from $f_C = 0.189$ to $f_C = 0.250$. Bailey et al. found that the O^{70} phase is stable for f_C over wider range of $f_C = 0.12-0.27$. The predicted minimum value of f_C is significantly greater than observed.

5. Diblock Copolymers

Our calculations of the phase behavior of an idealized ABC triblock copolymer and of a model ISO triblock copolymer both predict regions in which the O^{70} phase is stable that extends to the AB edge of the phase triangle. This implies that the O^{70} phase is also a stable phase of diblock copolymer melts. To emphasize this point, we show in Figure 12 the free energies per molecule of the G, S, C, and O^{70} phases, relative to that of L, for a diblock copolymer with equal statistical segment lengths and $\chi N = 13$, corresponding to AB edge of the phase triangle shown in Figure 3. Our calculations are such that the errors in the free energies per molecule are smaller than the width of the plotted lines in this figure—although the differences in free energy per molecule between O^{70} and competing G and L phases are less than $10^{-3}k_BT$, the calculations are converged to within $10^{-6}k_BT$. For $\chi N = 13$, the O^{70} phase is stable for $f_A = 0.418-0.422$.

No prior published calculations of the diblock phase map in SCFT have considered O^{70} as a candidate phase. Because our triblock phase maps indicate that the O^{70} phase is stable in the limit of an idealized diblock copolymer, we have calculated the diblock copolymer phase map for a block copolymer with equal statistical segment lengths. We have included the O^{70}, G, L, C, and S phases as candidate structures.

The relevant region of the resulting phase map for diblock copolymers is shown in Figure 13. The O^{70} network is found to be stable within a narrow range of compositions that borders the lamellar phase, for χN from 10.495 to 13.76. The O^{70} phase is stable in a weakly segregated region that overlaps and extends the weakly segregation end of the region in which the gyroid had previously been predicted to be stable. The existence of the O^{70} phase in the diblock phase map removes the L/G/C triple point that Matsen and Schick[36] had predicted to occur at $\chi N = 11.14$ and $f_A = 0.452$. The boundaries of the O^{70} phase meet at an L/G/O^{70} triple point and a C/G/O^{70} triple point. The values of χN and f_A at these triple points, as well as the unit cell parameters, are given in Table 5. Unlike the gyroid phase, the O^{70} phase appears to extend as a narrow sliver all the way down to the critical point at $\chi N = 10.495$ and $f_A = 0.5$. This feature, which is difficult to resolve in numerical SCFT, has been confirmed by Ranjan and Morse by considering the weak-segregation theory.[50]

Figure 14 shows the $\phi_A = \phi_B = 0.5$ isosurfaces as well as the gradients of density within those surfaces for both the A and B monomers with $f_A = 0.43$ and $\chi N = 12.0$. The minority A domain forms a network within a matrix of B. At these weak segregation strengths, the interfaces in this structure are diffuse; neither monomer exceeds 85% purity at any location within the unit cell.

Table 6 lists the components of the differences in free energy between the O^{70} phase and the neighboring lamellar and G phases at points along the intersection of the phase boundaries with the line $\chi N = 12$. For this system, we have subdivided the conformational free energy into contributions arising from

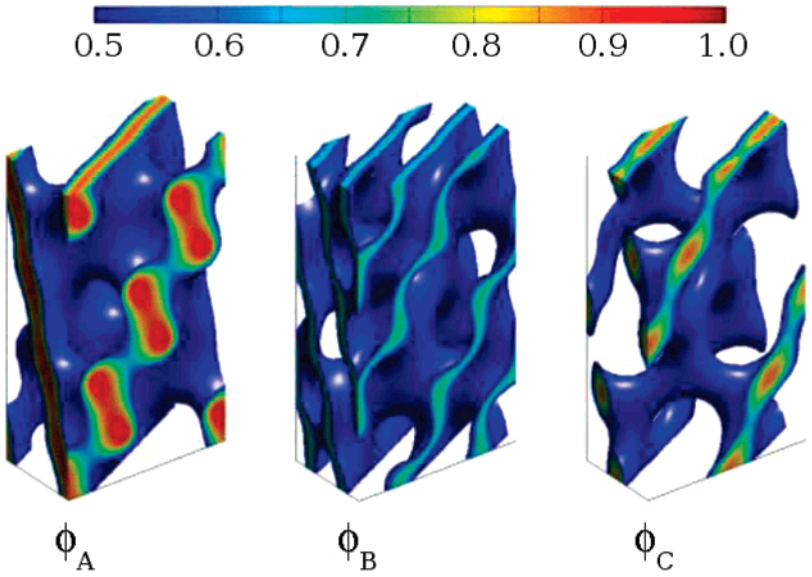

Figure 10. A(I), B(S), and C(O) domains in the O^{70} network of an ISO triblock, as predicted by SCFT. The isosurfaces are shown for each monomer at $\phi_\alpha = 0.5$. The morphology is core−shell-like, with an C network, a B shell, and an A matrix. The B domain is quite weakly segregated, never exceeding a volume fraction of 70%.

Table 4. Components of the Differences in Free Energies of the ISO O^{70} Phase and Those of the Surrounding Phases at Selected Boundary Points, in Units of k_BT per Molecule[a]

α	β	(f_A, f_B, f_C)	ΔF_{AB}	ΔF_{BC}	ΔF_{AC}	ΔF_{chain}
O^{70}	G_{CA}	(0.408, 0.382, 0.210)	−0.018 722	0.020 969	0.003 221	−0.005 468
	G_{CB}	(0.222, 0.568, 0.210)	−0.016 042	0.021 607	−0.013 051	0.007 486
	L_2	(0.406, 0.406, 0.188)	0.067 917	−0.100 121	0.015 259	0.0169 46
	L_3	(0.375, 0.375, 0.250)	0.056 290	−0.086 875	0.033 938	−0.003 352
	G^A	(0.238, 0.580, 0.182)	0.040 548	−0.035 229	0.005 099	−0.010 418

[a] G_{CA} represents the gyroid phase with a core of C in an A matrix, which is stable near the A-rich corner, while G_{CB} represents the network phase with a network of C in a B matrix, which is stable nearer the B-rich corner.

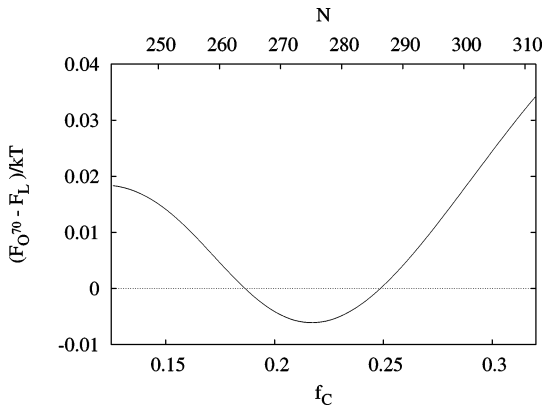

Figure 11. Free energy of the O^{70} phase relative to that of the L phase with increasing length of the C block at fixed length of the A and B blocks. The χ parameters are those of our base case for ISO. The O^{70} phase is the stable phase for values of f_C from 0.186 to 0.249.

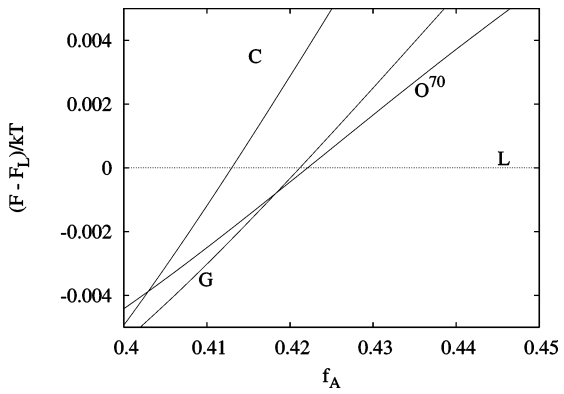

Figure 12. Free energies of the O^{70}, G, S, and C phases for a diblock copolymer at $\chi N = 13$, relative to that of the L phase.

stretching of the A and B blocks and from the entropy loss arising from localization of the joint near the AB interface, using the decomposition introduced by Matsen and Bates in eqs 7−10 of ref 40. Along the phase sequence $L \rightarrow O^{70} \rightarrow G$ that is traversed at this value of χN by increasing compositional asymmetry, both the $L \rightarrow O^{70}$ and $O^{70} \rightarrow G$ transition lead to increases in the AB interaction free energy, which are compensated by decreases in chain conformational free energy. In weakly segregated diblock copolymers, the A-core O^{70} phase thus has a lower AB core−matrix interaction free energy than the G phase, while the gyroid has a lower stretching free energy for both blocks. Because there is only one type of binary interaction in a diblock melt, our understanding of the competition between the O^{70} and G phases in weakly segregated AB diblocks is necessarily somewhat different from that suggested by Table 2 for ABC triblocks with $f_C < f_A < f_B$, in which we found that the A core O^{70} network is stabilized relative to the analogous G network by a favorable BC matrix−interstitial interaction.

In a recent paper,[51] Takenaka et al. have reported the identification of an O^{70} phase over a narrow temperature range near the order−disorder transition in a nearly symmetric poly(isoprene-*b*-styrene) diblock copolymer. The ratios of unit cell dimension required to index the peaks obtained in small-angle X-ray scattering are consistent with the predictions of SCFT, which are discussed in section 6. It is not clear from this

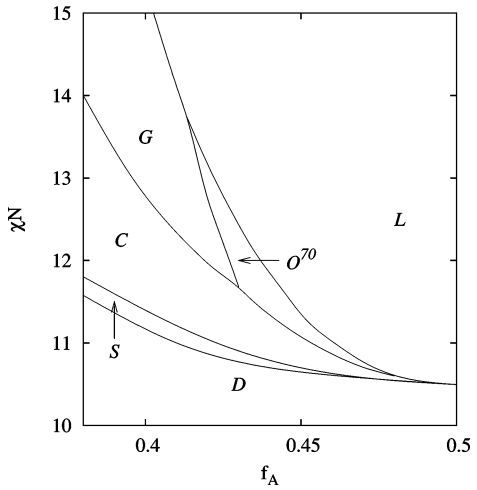

Figure 13. SCFT phase map of an idealized diblock copolymer with equal statistical segment lengths as a function of $f_A = 1 - f_B$ and χN. Only *G*, *S*, *C*, *L*, and O^{70} phases are considered as candidates.

Table 5. Thermodynamic and Unit Cell Parameters of the O^{70} Phase at the Triple Points of the Diblock Copolmer Phase Map Shown in Figure 13[a]

phases	χN	f_A	a/R_g	b/a	c/a
$L/G/O^{70}$	13.76	0.413	4.06	2.01	3.56
$C/G/O^{70}$	11.64	0.431	3.84	2.00	3.51

[a] Here, *a*, *b*, and *c* are the equilibrium orthorhombic unit cell dimensions, and $R_g = (Nb^2/6)^{1/2}$ is the radius of gyration.

preliminary report whether this is an equilibrium or a metastable structure.

6. The O^{70} Unit Cell

The orthorhombic unit cell of the equilibrium O^{70} structure exhibits a characteristic set of ratios (*a*:*b*:*c*) of the unit cell dimensions *a*, *b*, and *c*. The geometry of this characteristic unit cell is evident from the results of scattering experiments. In the small-angle X-ray scattering (SAXS) experiments of Epps et al.,[17] the three peaks of smallest scattering wave number in powder-pattern scattering intensity profiles nearly overlap. These three peaks correspond to the (004), (111), and (022) families of Bragg reflections. The peaks corresponding to the (004) and (022) directions, in particular, are indistinguishable even in high-resolution synchrotron SAXS data. The square magnitudes of the relevant sets of scattering wavevectors are

$$G^2_{(111)} = \frac{1}{a^2} + \frac{1}{b^2} + \frac{1}{c^2} \tag{3}$$

$$G^2_{(022)} = \frac{4}{b^2} + \frac{4}{c^2} \tag{4}$$

$$G^2_{(004)} = \frac{16}{c^2} \tag{5}$$

The (022) and (004) peak wavenumbers coincide if $c = \sqrt{3}b$. All three peaks coincide if and only if

$$(a{:}b{:}c) = (1{:}2{:}2\sqrt{3}) \tag{6}$$

or (*a*:*b*:*c*) = (1:2:3.464). The observation that these three peaks overlap in orientationally averaged scattering thus implies a unique set of ratios of the three unit cell parameters.

Our SCFT predictions for the equilibrium unit-cell parameters of the O^{70} phase in both triblock and diblock copolymers coincide closely with eq 6 and thus with the SAXS data collected by Epps et al.[17] The calculated unit cell parameters for the diblock copolymer at the $L/G/O^{70}$ and $C/G/O^{70}$ triple points, which are listed in Table 5, are very close to these ratios. Furthermore, for diblocks these ratios are found to asymptotically approach the values given in eq 6 as the critical point is approached in the limit $\chi N \rightarrow 10.495$ and $f_A \rightarrow 0.5$. At predicted ratios of unit cell parameters for an ISO triblock copolymer are shown in Figure 15 along the line $f_C = 0.21$. The ratios b/a and (particularly) c/b are extremely close to 2 and $\sqrt{3}$, respectively, leading to nearly perfect overlap of magnitudes of the (004) and (022) reciprocal vectors. The ratio c/a deviates slightly more from $2\sqrt{3}$ but remains within 2% of this value over the range of compositions in which the O^{70} phase is stable.

The reasons for the coincidence of the first three scattering peaks in weakly segregated O^{70} structures may be understood in the context of a Landau weakly segregation theory similar to that constructed for diblock copolymer melts by Leibler.[35] This weak-segregation theory has recently been extended to include the O^{70} phase by Ranjan and Morse.[50] The disordered phase becomes unstable at a spinodal with respect to density modulations with a nonzero wave number q^*. Weakly segregated ordered phases may be approximated by a single-wavenumber expansion as superpositions of plane waves with wavevectors of equal magnitude $|\mathbf{q}| = q^*$. The O^{70} phase may be constructed from the 14 wavevectors contained in the (111), (022), and (004) families of reflections, for a unit cell in which these wavevectors all have magnitude of q^*. Ranjan and Morse found, within the context of this theory, that an O^{70} phase with this special unit cell is stable in a narrow sliver between the lamellar and hexagonal phases that extends to the critical point.

Bailey et al.[16] originally proposed a simplified geometrical model for the O^{70} phase, which yields a unit cell different from that discussed above. In this simplified model, the O^{70} phase is idealized as a network of equal length struts of the "core" component connected by nodes at which three struts meet with equal 120° angles. Figure 16 illustrates the model. This model has only two parameters: the length of one strut and the angle θ formed between the projection onto the *ab* plane of the struts that are not parallel to the *c* axis. The unit-cell parameters of an O^{70} network based on this model are

$$(a{:}b{:}c) = (1{:}\cot\theta{:}\sqrt{3}\csc\theta) \tag{7}$$

This is equivalent to a requirement that $c^2 = 3(a^2 + b^2)$, where $a/b = \tan\theta$. Bailey et al.[16] suggested that the shear angle varies around an average value of $2\theta = 60°$. For $2\theta = 60°$, the ratios of unit cell parameters are $(a{:}b{:}c) = (1{:}\sqrt{3}{:}2\sqrt{3})$. No choice of shear angle will produce unit-cell parameters in the ratio $(1{:}2{:}2\sqrt{3})$ given in eq 6, for which $c^2/(a^2 + b^2) = 12/5$.

An *Fddd* with a slightly different unit cell was identified, independently of our work, in a theoretical study of the kinetics of phase transitions in diblock copolymer melts by Yamada, Nonomura, and Ohta.[52−54] The work of this group is based on an approximate weak-segregation theory in which the monomer concentration fields in all structures of interest are represented as superpositions of a limited number of plane waves. Specifically, these authors have considered structures that can be constructed as superpositions of plane waves in the {211} and {022} families of reciprocal lattice vectors of a cubic crystal. This choice of basis functions allowed them sufficient freedom to represent the lamellar, hexagonal, and gyroid phases and

Table 6. Components of the Differences in Free Energy between the O^{70} Phase and the *G* and *L* Phases in AB Diblock Copolymers with $b_A = b_B$, at Points along the O^{70}–*L* and O^{70}–*G* Phase Boundaries at Which $\chi N = 12$[a]

α	β	(f_A, f_B)	ΔF_{AB}	ΔF_A	ΔF_B	ΔF_J
O^{70}	*L*	(0.437, 0.563)	0.025 916	−0.011 936	−0.011 919	−0.002 128
	G	(0.427, 0.573)	−0.004 596	0.001 818	0.001 982	0.000 853

[a] Here ΔF_{AB} is the difference in binary interaction free energy, ΔF_A and ΔF_B are differences in the conformational free energies of the A and B blocks, respectively, and ΔF_J is a difference in the translational free energy arising from localization of the AB junction, as defined in ref 40.

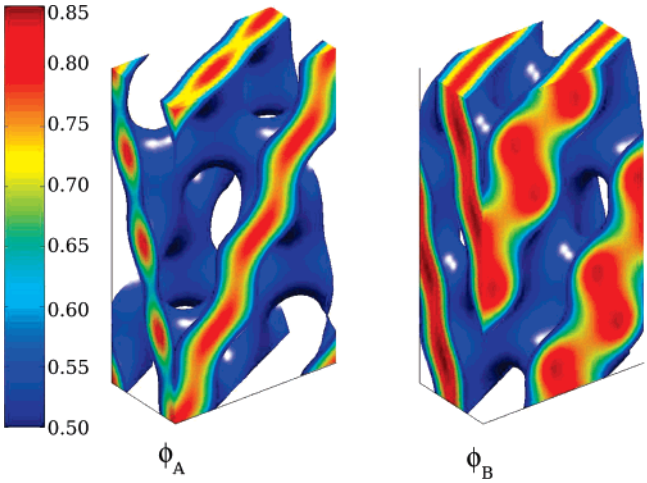

Figure 14. $\phi_A = \phi_B = 0.5$ isosurfaces as well as the gradients of density within the surface for A and B monomers for an O^{70} morphology of a diblock copolymer melt with $f_A = 0.43$, $\chi N = 12$, and $b_A = b_B$.

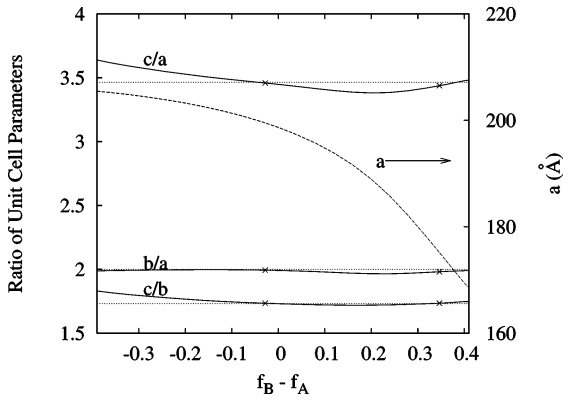

Figure 15. Ratios of unit-cell parameters *b*/*a*, and *c*/*a*, and *b*/*c* (solid lines) and the absolute magnitude of *a* in Å (dashed line) for our base-case ISO triblock with $\chi_{AB}N = 11.0$, $\chi_{BC}N = 14.2$, and $\chi_{AC}N = 45.8$, along the line $f_C = 0.21$. The O^{70} phase boundaries are marked by crosses. The ratios $1{:}2{:}2\sqrt{3}$) are shown by dotted lines.

yields phase boundaries for transitions between these phases that are similar to those predicted by SCFT. By adding a third set of plane waves, they were also able to represent the BCC phase. Among the locally stable structures that they identified was one with *Fddd* symmetry, with isosurfaces of the same topology as those obtained here for the *Fddd* phase. This structure was initially reported to be a metastable structure,[52,53] which was found to appear in Langevin simulations as a transition state during transitions from the gyroid to the lamellar phase, lamellar to gyroid, and from hexagonal to gyroid phase.[52] A subsequent reexamination of the equilibrium phase diagram for this model,[54] in which the authors included two more families of plane waves in the Fourier expansion, {310} and {400}, showed that this structure is actually stable within a very small region of parameter space (much smaller than that shown in Figure 13) near the point at which the gyroid, hexagonal, and lamellar phases have equal free energies.

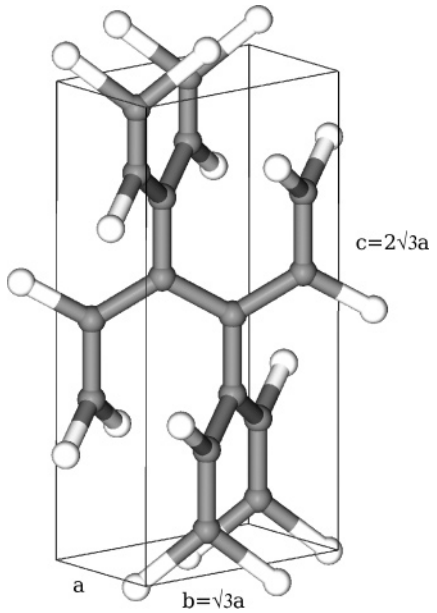

Figure 16. A ball and stick model of the O^{70} phase, constrained such that each stick is of fixed length, with a shear angle of 60°.

The *Fddd* structure considered by Yamada et al.[52,53] was constructed from a superposition of 12 of the 24 {211} reciprocal lattice vectors and two {022} vectors of a cubic lattice. This yields a set of 14 wavevectors, but one in which the two wavevectors from the {022} family have a magnitude that is larger by a factor of $\sqrt{4/3}$ than the other 12. This set of 14 peaks can also be represented on an orthorhombic lattice by associating the {022} reciprocal vectors of the cubic lattice with the {004} reciprocal vectors of the orthorhombic lattice and the 12 relevant {211} vectors of the cubic lattice with the {022} and {111} reciprocal vectors of the orthorhombic lattice. The *a*, *b*, and *c* axes of the orthorhombic unit cell are aligned, e.g., parallel to the $(0\bar{1}1)$, (100), and (011) directions of the cubic cell, respectively. The requirements that the magnitude of the orthorhombic {111} and {022} reciprocal vectors be equal, and that the magnitude of the {004} reciprocal vector be larger by a factor of $\sqrt{4/3}$, imply that the orthorhombic unit cell must have dimensions

$$(a{:}b{:}c) = (1{:}3/\sqrt{2}{:}3) \tag{8}$$

or $(a{:}b{:}c) = (1.0{:}2.12{:}3.0)$. The *Fddd* structure considered by Yamada et al. is thus based on deformed version of the equilibrium *Fddd* unit cell, in which the *c* axis is shortened by 13.4%. This deformation allows the establishment of an epitaxial relationship between the gyroid and *Fddd* structures. This structure was presumably found to be stable over a substantially smaller region than found here for the optimal *Fddd* unit cell as a result of the increase in free energy caused by this deformation.

7. Sensitivity Analysis

The experimentally observed phase map, shown in Figure 1, and our SCFT phase map for ISO, shown in Figure 8, agree

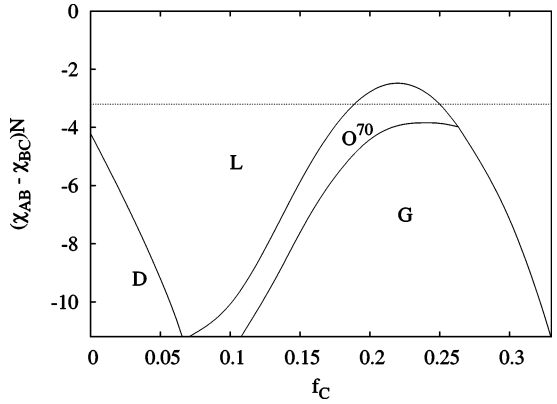

Figure 17. $(\chi_{AB} - \chi_{BC})-f_C$ phase map of an ISO triblock copolymer along the $f_A = f_B$ isopleth, with $\chi_{AC}N = 45.8$, $(\chi_{BC} + \chi_{AB})N = 25.2$, $b_A = 6.0$ Å, $b_B = 5.5$ Å, and $b_C = 7.8$ Å. The dotted line at $(\chi_{AB} - \chi_{BC})N = -3.2$ represents the intersection of this phase map with the base-case phase triangle in Figure 8.

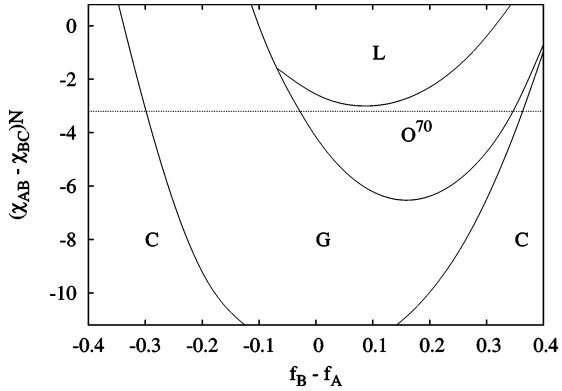

Figure 18. $(\chi_{AB} - \chi_{BC})-(f_B - f_A)$ phase map of an ISO triblock copolymer along the $f_A = f_B$ isopleth, with $\chi_{AC}N = 45.8$, $(\chi_{BC} + \chi_{AB})N = 25.2$, $b_A = 6.0$ Å, $b_B = 5.5$ Å, and $b_C = 7.8$ Å. The dotted line at $(\chi_{AB} - \chi_{BC})N = -3.2$ represents the intersection of this phase map with the base-case phase triangle in Figure 8.

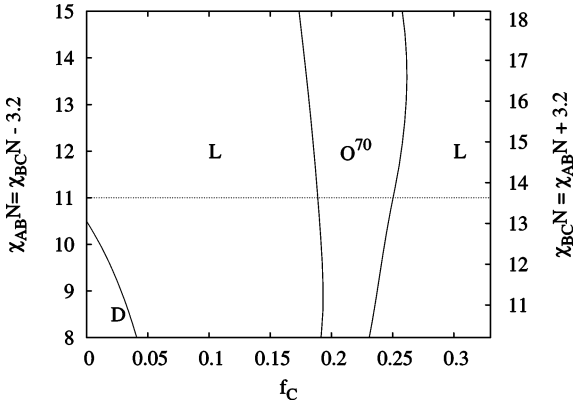

Figure 19. $(\chi_{AB} - \chi_{BC})-f_C$ phase map of an ISO triblock along the $f_A = f_B$ isopleth, with $\chi_{AC}N = 45.8$, $(\chi_{AB} - \chi_{BC})N = -3.2$, $b_A = 6.0$ Å, $b_B = 5.5$ Å, and $b_C = 7.8$ Å. The dotted line at $\chi_{AB}N = 11.0$ represents the intersection of this phase diagram with the base-case phase triangle in Figure 8.

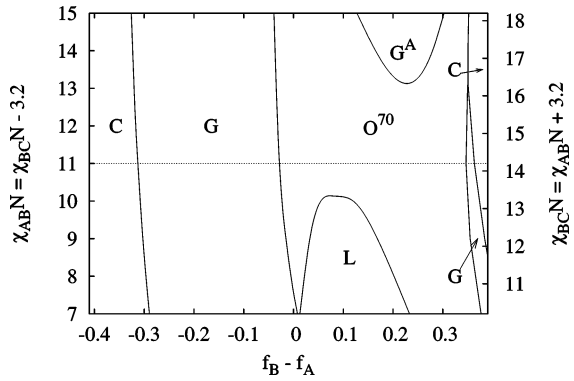

Figure 20. $(\chi_{AB} - \chi_{BC})-(f_B - f_A)$ phase map of an ISO triblock along the $f_C = 0.21$ isopleth, with $\chi_{AC}N = 45.8$, $\chi_{BC}N = \chi_{AB}N + 3.2$, $b_A = 6.0$ Å, $b_B = 5.5$ Å, and $b_C = 7.8$ Å. The dotted line at $\chi_{AB}N = 11.0$ represents the intersection of this phase diagram with the base-case phase triangle in Figure 8.

qualitatively. In both phase maps, the O^{70} phase is stable around the $f_A = f_B$ isopleth and is bordered by the L, G, and G^A phases. The agreement is not quantitative, however; the precise locations of phase boundaries differ significantly. This is not surprising, particularly in light of the substantial uncertainty in our choice of literature values for the ISO interaction parameters and the substantially different phase maps obtained in sections 3 and 4 for slightly different sets of parameters. A more complete understanding of the phase behavior of this class of systems thus requires some understanding of the sensitivity of the predicted phase map to modest changes in the χ parameters. Such a sensitivity analysis also helps us to understand to what extent the discrepancies between our predictions for ISO and the experimental phase map might be reasonably attributed to errors in our chosen χ parameters and to what extent they must be attributed to limitations of SCFT itself.

In this section, we thus explore the sensitivity of the predicted phase boundaries for our ISO triblock copolymer model to variations in the three binary interaction parameters. We consider variations of all three parameters around a base case considered in section 4, in which $\chi_{AB}N = 11.0$, $\chi_{AC}N = 45.8$, and $\chi_{BC}N = 14.2$. We have considered three independent variations of the interaction parameters: (1) varying the difference $(\chi_{AB} - \chi_{BC})$ while keeping χ_{AC} and the sum $(\chi_{AB} + \chi_{BC})$ fixed; (2) varying the sum $(\chi_{AB} + \chi_{BC})$ while keeping χ_{AC} and the difference $(\chi_{AB} - \chi_{BC})$ fixed; (3) varying χ_{AC} while keeping χ_{AB} and χ_{BC} fixed. We have explored the effect of all three variations along a line $f_A = f_B$ and the first two along a line with fixed $f_C = 0.21$ isopleth. Both lines are chosen to cut through the region of predicted O^{70} stability. The resulting phase maps are shown in Figures 17−21. In each of these phase maps, the choice of parameters corresponding to the base case studied in section 4 is shown as a dotted line.

Most of the trends found in this numerical sensitivity analysis can be rationalized by considering the values of the differences ΔF_{ij} in binary interaction free energies between competing phases. It is straightforward to show that the derivative of the free energy difference $\Delta F = F^{\alpha} - F^{\beta}$ between phases α and β with respect to changes in a single interaction parameter χ_{ij}, at fixed composition and fixed statistical segment lengths, is given exactly by

$$\chi_{ij}\frac{\partial \Delta F}{\partial \chi_{ij}} = \Delta F_{ij} \tag{9}$$

where $\Delta F_{ij} = F_{ij}^{\alpha} - F_{ij}^{\beta}$ is the difference between the binary ij interaction free energies of phases α and β. This identity simply tells us that increasing χ_{ij} will always favor the phase for which the ij interaction free energy is lower. The relevant differences in binary interaction free energies between the ISO O^{70} phase and its competitors are given in Table 4.

Figures 17 and 18 show the phase maps produced by varying $(\chi_{AB} - \chi_{BC})$ at fixed χ_{AC} and fixed $(\chi_{AB} + \chi_{BC})$, along the line $f_A = f_B$ and $f_C = 0.21$, respectively. The base case seems to be a nearly optimal choice for stabilizing a large O^{70} phase window. Along either isopleth, we see that a decrease in the $(\chi_{AB} - \chi_{BC})$

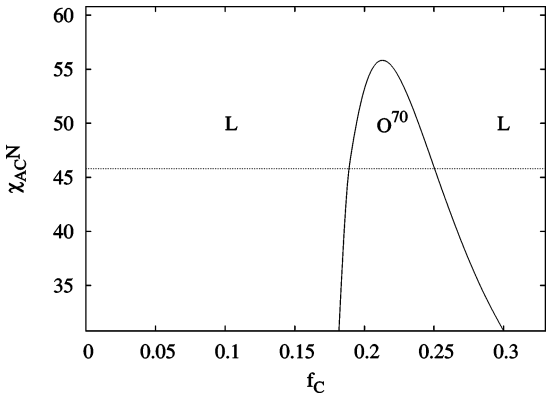

Figure 21. χ_{AC}−f_C for an ISO triblock along the $f_A = f_B$ isopleth, with $\chi_{AB}N = 11.0$, $\chi_{BC}N = 14.2$, $b_A = 6.0$ Å, $b_B = 5.5$ Å, and $b_C = 7.8$ Å. The dotted line at $\chi_{AC}N = 45.0$ represents the intersection of this phase diagram with the base-case phase triangle in Figure 8.

would drive a transition from O^{70} to L, while a further increase would force a transition from O^{70} to G. Because the base value of $\chi_{AB}N = 11$ for the AB interaction is close to the critical value of $\chi_{AB}N = 10.495$ for a symmetric diblock, a disordered phase appears in Figure 17 near $f_C = 0$ for large values of ($\chi_{AB} - \chi_{BC}$).

We next consider variations in ($\chi_{AB} + \chi_{BC}$) at fixed χ_{AC} and ($\chi_{AB} - \chi_{BC}$). Figures 19 and 20 are the corresponding phase maps along the $f_A = f_B$ isopleth and the $f_C = 0.21$ isopleth, respectively. The phase boundaries along the $f_A = f_B$ isopleth are comparatively insensitive to this variation, whereas the phase boundaries along the $f_C = 0.21$ are more strongly influenced. As ($\chi_{AB} + \chi_{BC}$) becomes larger, the G^A phase becomes stable, crowding out O^{70}; indeed, at $\chi_{AB}N = 13.5$ and $\chi_{BC}N = 16.7$, SCFT predicts the phase sequence $G \rightarrow O^{70} \rightarrow G^A$ along the $f_C = 0.21$ isopleth. This is the phase sequence observed for ISO, as presented in Figure 1.

Finally, we vary χ_{AC} at fixed χ_{AB} and χ_{BC}. For systems with sharp AB and AC interfaces, we would expect almost no dependence of the phase boundaries upon this parameter, as found by Matsen[29] in more strongly segregated systems, because there would be almost no contact between A and C monomers. For the more weakly segregated structure considered here, however, we find that as χ_{AC} increases, the O^{70} window along the $f_A = f_B$ isopleth narrows, closing completely at $\chi_{AC}N \approx 55$, as shown in Figure 21. The lamellar phase is stabilized by increasing χ_{AC} because, as shown in Table 4, the lamellar phase has a smaller AC interaction energy than the O^{70} phase.

8. Conclusions

We have used SCFT to study the phase behavior of nonfrustrated ABC triblock copolymers, with $\chi_{AC} \gg \chi_{AB} \sim \chi_{BC}$. These systems tend to form phases in which the B phase is continuous, with no direct interface between A and C domains. The systems studied here have modest interactions between AB and BC monomer pairs, however, leading to rather broad AB and BC interfaces and to some residual interaction of A and C monomers within the ordered phases. We have considered both a thermodynamically symmetric model with $\chi_{AB} = \chi_{BC}$ and a slightly asymmetric model with parameters chosen to mimic, as best we can, those of ISO.

In the symmetric model, with $\chi_{AB} = \chi_{BC}$, the center of the phase map is dominated by a large lamellar region. The A- and C-rich corners, in which an end-block is the majority component, exhibit core−shell sphere, cylinder, and gyroid morphologies in which the minority end-block forms a core domain similar to that found in an analogous diblock copolymer structure. In the B-rich corner, we find regions of sphere, cylinder, gyroid, and O^{70} phases near the AB and/or BC diblock edges. These structures may be described qualitatively core/matrix/interstitial structures, in which, in the region $f_C < f_A < f_B$, an A block forms a core domain similar to that of the corresponding diblock copolymer phase and the C block segregates into an "interstitial" domain within a B matrix. Along the line $f_A = f_C$, this model exhibits an alternating sphere and alternating gyroid phase, in which the "core" and "interstitial" domains have a similar topology. The behavior along the line $f_A = f_C$ is consistent with that found previously by Matsen in systems with $\chi_{AB} = \chi_{BC}$ and $f_A = f_C$, except for the absence for the parameters chosen here of the alternating cylinder phase that was found by Matsen, which was observed experimentally by Mogi et al.

In the model with $\chi_{AB} = \chi_{BC}$, the region of stability of the O^{70} phase in the B-rich corner grows at the expense of a competing gyroid phase as the size of the minority end-block is increased, because the O^{70} phase provides a lower free energy of interaction between the matrix and interstitial block and (in such a weakly segregated system) also between the end-blocks. We suspect that the role of the interaction between mid- and end-blocks is general: in both of the models considered here, when a gyroid and O^{70} phase with a C core compete, the O^{70} phase is favored by a lower free energy of interaction between the matrix B block and the interstitial A block, corresponding to a smaller interface between the matrix and interstitial domains. The G^A phase is in turn favored over the O^{70} phase with a C core by a yet lower AB interaction. In this sense, the O^{70} phase in ABC triblocks may be considered as a natural intermediate between the gyroid and alternating gyroid phases.

Both of the models studied here exhibit a critical point in the B-rich corner, of the type predicted by Erukhimovich for systems that undergo an *AC* modulation. Phase behavior near this critical point is reminiscent of that predicted near $\chi N = 10.495$ and $f_A = 1/2$ in diblock copolymers: the magnitude of the periodic modulation of composition vanishes continuously as the critical point is approached by varying composition within any of several ordered phase, and several phase boundaries converge at the critical point. In the model with $\chi_{AB} = \chi_{BC}$, the critical point appears along the line $f_A = f_C$, as the result of a symmetry analogous to that which requires the critical point of an idealized diblock copolymer to lie along the line $f_A = 1/2$.

The most important difference between the model of ISO studied in section 4 and the idealized model of section 3 is the use in the ISO model of a slightly larger value of $\chi_{BC}N = 14.2$ and a smaller value of $\chi_{AB}N = 11.0$ than the value $\chi_{AB}N = \chi_{BC}N = 13$ used in section 3. This modest asymmetry causes significant change in the phase map, by causing a sequence of G and O^{70} network structures with C core domains to become stable across a band that connects the BC edge to the A-rich corner. The predicted phase map for this model agrees semi-quantitatively with that obtained by Epps et al.[17]

Our results for ABC triblocks copolymer led us to reexamine the diblock copolymer phase map. The O^{70} phase was found to be stable in diblock copolymers within a narrow weakly segregated region that overlaps the previously predicted region of stability of the gyroid phase and extends the region of stability of these two network phases to the critical point. The reasons for the stability of a very weakly segregated O^{70} phase in diblock copolymer melts appear to be best understood within the context of weak-segregation theory.[50]

The predicted dimensions of the unit cell of the O^{70} phase in the relatively weakly segregated triblock and diblock copolymer

melts studied here have ratios very close to a special set of values $(a:b:c) = (1:2:2\sqrt{3})$ for which the primary (004), (022), and (111) families of reciprocal vectors have equal magnitudes. The unit cell shape predicted with SCFT agrees well with that obtained in SAXS experiments on ISO, in which the three corresponding scattering peaks overlap. Neither our SCFT predictions nor the SAXS results are adequately described by the model proposed by Bailey et al. of a network of equal-length struts connected at equal angles at 3-fold nodes.

The size and location of the predicted O^{70} phase window in ISO are found to depend strongly on the difference between the input values of χ_{AB} and χ_{BC}. For smaller values of this difference, an *L* phase would be stable; for larger values than that used here; a *G* network would become stable instead of an O^{70} network. Our analysis suggests that it is probably not possible to dramatically improve the extent of agreement between SCFT and the experimental results of Epps et al. by further refinement of the χ parameters.

The calculations presented here are restricted to rather weakly segregated structures, using parameters chosen to mimic the initial experimental studies on ISO systems with accessible order−disorder transitions.[16,17] In a subsequent experimental study of ISO samples of substantially higher molecular weight,[55] poorly ordered but apparently multiply continuous structures were observed by transmission electron microscopy in the composition range in which well-ordered O^{70} structures were identified in lower molecular weight samples. Future theoretical work will examine whether the O^{70} phase remains thermodynamically stable in more strongly segregated ABC triblocks or whether, as found for AB diblocks, it is stable only in weakly segregated systems.

Acknowledgment. This work was supported by National Science Foundation (NSF) grant DMR-0220460 (support for J. Qin) and by the NSF MRSEC program under Award DMR-0243589 (support for C. Tyler), using computer resources provided by both the Minnesota Supercomputer Institute and the UMN MRSEC.

References and Notes

(1) Bailey, T. S. Morphological behavior spanning the symmetric AB and ABC block copolymer states. Thesis, University of Minnesota, 2001.
(2) Auschra, C.; Stadler, R. *Macromolecules* **1993**, *26*, 2171−2174.
(3) Stadler, R.; Auschra, C.; Beckmann, J.; Krappe, U.; Voight-Martin, I.; Leibler, L. *Macromolecules* **1995**, *28*, 3080−97.
(4) Breiner, U.; Krappe, U.; Stadler, R. *Macromol. Rapid Commun.* **1996**, *17*, 567−575.
(5) Breiner, U.; Krappe, U.; Abetz, V.; Stadler, R. *Macromol. Chem. Phys.* **1997**, *198*, 1051−1083.
(6) Breiner, U.; Krappe, U.; Jakob, T.; Abetz, V.; Stadler, R. *Polym. Bull.* **1998**, *40*, 219−226.
(7) Ott, H.; Abetz, V.; Alstadt, V. *Macromolecules* **2001**, *34*, 2121−2128.
(8) Brinkmann, S.; Stadler, R.; Thomas, E. L. *Macromolecules* **1995**, *28*, 6566−6572.
(9) Krappe, U.; Stadler, R.; Voigt-Martin, I. *Macromolecules* **1995**, *28*, 4558−4561.
(10) Balsamo, V.; Glydenfeldt, F. V.; Stadler, R. *Macromolecules* **1999**, *32*, 1226−1232.
(11) Hueckstadt, H.; Gopfert, A.; Abetz, V. *Polymer* **2000**, *41*, 2121−2128.
(12) Abetz, V.; Goldacker, T. *Macromol. Rapid Commun.* **2000**, *21*, 16−34.
(13) Mogi, Y.; Mori, K.; Kotsuji, H.; Matsushita, Y.; Noda, I.; Han, C. C. *Macromolecules* **1993**, *26*, 5169−5173.
(14) Mogi, Y.; Nomura, M.; Kotsuji, H.; Ohnishi, K.; Matsushita, Y.; Noda, L. *Macromolecules* **1994**, *27*, 6755−66760.
(15) Matsushita, Y.; Suzuki, J.; Seki, M. *Physica B* **1998**, *248*, 238−242.
(16) Bailey, T. S.; Hardy, C. M.; Epps, T. H.; Bates, F. S. *Macromolecules* **2002**, *35*, 7007−7017.
(17) Epps, T. H.; Cochran, E. W.; Hardy, C. M.; Bailey, T. S.; Waletzko, R. S.; Bates, F. S. *Macromolecules* **2004**, *36*, 2873−2881.
(18) Chatterjee, J.; Jain, S.; Bates, F. S. *Macromolecules* **2007**, *40*, 2882−2896.
(19) Hueckstadt, H.; Goldacker, T.; Gopfert, A.; Abetz, V. *Macromolecules* **2000**, *33*, 3757−3761.
(20) Matsushita, Y.; Tamura, M.; Noda, I. *Macromolecules* **1992**, *27*, 3680−3682.
(21) Shefelbine, T.; Vigild, M.; Matsen, M.; Hajduk, D.; Hillmyer, M.; Cussler, E.; Bates, F. *J. Am. Chem. Soc.* **1999**, *121*, 8457−8465.
(22) Cochran, E. W.; Bates, F. S. *Phys. Rev. Lett.* **2004**, *93*, 087802.
(23) Nakazawa, H.; Ohta, T. *Macromolecules* **1993**, *26*, 5503−5511.
(24) Zheng, W.; Wang, Z. G. *Macromolecules* **1995**, *28*, 7215−7223.
(25) Phan, S.; Fredrickson, G. H. *Macromolecules* **1997**, *31*, 59−63.
(26) Ohta, T.; Kawasaki, K. *Macromolecules* **1986**, *19*, 2621−2632.
(27) Ohta, T.; Kawasaki, K. *Macromolecules* **1990**, *23*, 2413−2414.
(28) Tyler, C. A.; Morse, D. C. *Phys. Rev. Lett.* **2005**, *94*, 208302.
(29) Matsen, M. W. *J. Chem. Phys.* **1998**, *108*, 785−796.
(30) Tang, P.; Qui, F.; Zhang, H.; Yang, Y. *Phys. Rev. E* **2004**, *69*, 031803.
(31) Xia, J.; Sun, M.; Zhang, H.; Yang, Y. *Macromolecules* **2005**, *38*, 9324−9332.
(32) Jiang, Y.; Yan, X.; Liang, H.; Shi, A.-C. *J. Phys. Chem. B* **2005**, *109*, 21047−21055.
(33) Erukhimovich, I. Y.; Abetz, V.; Stadler, R. *Macromolecules* **1997**, *30*, 7435−7443.
(34) Erukhimovich, I. Y. *Eur. Phys. J. E* **2005**, *18*, 383−406.
(35) Leibler, L. *Macromolecules* **1980**, *13*, 1602−1617.
(36) Matsen, M.; Schick, M. *Phys. Rev. Lett.* **1994**, *72*, 2660−2663.
(37) Tyler, C. A.; Morse, D. C. *Macromolecules* **2003**, *36*, 8184−8188.
(38) Well, A. F. *Three-Dimensional Nets and Polyhedra;* Wiley Monographs in Crystallography; Wiley-Interscience: New York, 1977.
(39) Rasmussen, K.; Kalosakas, G. *J. Polym. Sci., Part B* **2002**, *40*, 1777−1783.
(40) Matsen, M.; Bates, F. *J. Chem. Phys.* **1997**, *106*, 2436−2448.
(41) Maurer, W. M.; Bates, F. S.; Lodge, T. P.; Almdal, K.; Mortensen, K.; Fredrickson, G. *J. Chem. Phys.* **1998**, *108*, 2989−3000.
(42) Hanley, K. J.; Lodge, T. P. *J. Polym. Sci., Part B* **1998**, *36*, 3101−3113.
(43) Hashimoto, T.; Ijichi, Y.; Fetters, L. J. *J. Chem. Phys.* **1988**, *89*, 2463−2472.
(44) Balsara, N. P.; Fetters, L. J.; Hadjichristidis, N.; Lohse, D. J.; Han, C. C.; Graessley, W. W.; Krishnamoorti, K. *Macromolecules* **1992**, *24*, 6137−6147.
(45) Lin, C. C.; Jonnalagadda, S. V.; Kesani, P. K.; Dai, H. J.; Balsara, N. P. *Macromolecules* **1994**, *27*, 7769−7780.
(46) Frielinghaus, H.; Hermsdorf, N.; Almdal, K.; Mortensen, K.; Messe, L.; Corvazier, L.; Fairclough, J. P. A.; Ryan, A. J.; Olmsted, P. D.; Hamley, I. W. *Europhys. Lett.* **2001**, *53*, 680−686.
(47) Frielinghaus, H.; Pedersen, W. B.; Larsen, P. S.; Almdal, K.; Mortensen, K. *Macromolecules* **2001**, *34*, 1096−1104.
(48) Floudas, G.; Ulrich, R.; Wiesner, U. *J. Chem. Phys.* **1999**, *110*, 652−663.
(49) Cochran, E. W.; Morse, D. C.; Bates, F. S. *Macromolecules* **2003**, *36*, 782−792.
(50) Ranjan, A.; Morse, D. *Phys. Rev. E* **2006**, *74*, 011803.
(51) Takenaka, M.; Wakada, T.; Akasaka, S.; Nishitsubji, S.; Saijo, K.; Shimizu, H.; Kim, M.; Hasegawa, H. *Macromolecules* **2007**, published on Web, DOI: 10.1021/ma070739u.
(52) Yamada, K.; Nonomura, M.; Ohta, T. *Macromolecules* **2004**, *37*, 5762−5777.
(53) Yamada, K.; Nonomura, M.; Saeki, A.; Ohta, T. *J. Phys.: Condens. Matter* **2005**, *17*, 4877−4887.
(54) Yamada, K.; Nonomura, M.; Ohta, T. *J. Phys.: Condens. Matter* **2006**, *18*, L421−L427.
(55) Epps, T.; Bates, F. *Macromolecules* **2006**, *39*, 2676−2682.

MA062778W